ELECTROCHEMICAL BIOSENSORS FOR CLINICAL ANALYSIS OF MICRO RNA BIOMARKERS OF CANCER

By
Esther Tanumihardja

GRADUATION REPORT

Submitted to
Hanze University of Applied Science Groningen

in partial fulfillment of the requirements
for the degree of

Fulltime Honours Bachelor Advanced Sensor Applications

2015

ABSTRACT

ELECTROCHEMICAL BIOSENSORS FOR CLINICAL ANALYSIS OF MICRO RNA BIOMARKERS OF CANCER

By

Esther Tanumihardja

Genetic assays are very useful tools for clinical diagnostics and therapeutics. This thesis addresses the development of electrochemical microRNA genosensor, envisioned to be used as a clinical diagnostic tool. Dysregulation of numerous microRNAs have been reported to be closely associated to diseases. This makes them valuable biomarkers for minimally-invasive diagnostics. However, detection of microRNA is challenging, especially in the minute amount of circulating microRNAs. The research focused on achieving a reliable and sensitive sensing mechanism for circulating microRNA biomarkers of hypoxia. The approach can potentially be a rapid and less-laborious alternative to the traditional immunohistochemistry assay.

Based on review of different genosensor approaches, a model based on conformational change signalling was conceptualized, which then was put into experimental testing using synthetic nucleic acid polymers and electrochemistry (voltammetry) interrogation methods. Experimental results revealed that a robust, reliable genosensor signalling could be achieved the proposed model. However, required detection limit was not achieved in experimental data, and thus still need further work for genosensor's clinical application.

DECLARATION

I hereby certify that this report constitutes my own product, that where the language of others is set forth, quotation marks so indicate, and that appropriate credit is given where I have used the language, ideas, expressions or writings of another.

I declare that the report describes original work that has not previously been presented for the award of any other degree of any institution.

Signed,

Esther Tanumihardja

ACKNOWLEDGEMENTS

Contents

List of Figures

List of Tables

Chapter 1
Rationale

Malignant tumour, or cancer, is a non-communicable disease where a group of cells undergo uncontrolled proliferation, which lead eventually to growth of abnormal tissues. This proliferation, more often than not, results in some degree of hypoxia [1]. Incidences of hypoxia have been reported in almost all solid tumour cases [2].

Generally, hypoxia is a state of reduced oxygen availability in one site when compared to its normal/healthy counterpart. In the case of (solid) tumours, this is initially caused by the limitation of oxygen diffusion in avascular tumours when the cells outgrow its oxygen supply. The tissues might prompt angiogenesis, creating new microvasculature. It was reported, however, that the new microvasculature is commonly defective, thus not allowing correction of the oxygen deficit, ensuing chronic hypoxia [3], [4].

Chronic hypoxic microenvironment affects the biology of both tumour and immune cells significantly. Whereas acute hypoxia leads to short-lived responses (caused by modifications of existing proteins), chronic hypoxia leads to more enduring responses caused by modifications of gene expressions [5]. Both pro-apoptosis and pro-survival oncogenic phenotype changes have been reported as hypoxia-induced responses [6]. Discrepancies still exist in the underlying mechanisms leading to such responses. Nevertheless, in pro-survival response, tumour's invasiveness is increased, metastasis is promoted, as well as resistance to therapies (radiotherapy, phototherapy, chemotherapy, and immunotherapy) [3]. Withal, hypoxia is often times strongly correlated to poor prognosis of the disease [7]. Therefore detection of hypoxia is of major concern both in cancer diagnosis, as well as treatment.

Detection of hypoxia is a challenge. There are no definite clinical signs of hypoxia to begin with. Physiological or biochemical assessment is required for diagnosis. Since hypoxia is a strictly localized condition, applicability of global parameters is downplayed. There are a number of detection methods employed in tumour hypoxia detection nowadays [7], the most common one being immunohistochemical analysis of invasively harvested tissue. Ultimately, hypoxia is diagnosed in comparison with tissues' healthy counterpart [7], [8].

Immunohistochemistry is a technique using antibodies to dye specific protein of interest in a tissue. A (dye) label is tagged to the said antibodies. Through specific binding, the protein of interest will in turn be stained by the dye. Their presence, therefore, can be observed by means of microscope for diagnosis, based on the intensity of the staining, number of stained cells, localisation of stain within tissue. The whole process takes typically days, including processing the tissue, cutting the slides, and staining [9]. Thus apart from the invasiveness, the approach is also highly time and labour consuming. Consequently, another detection approach is highly desirable.

This project contributes to the development of a rapid biosensor in detecting hypoxia microRNA biomarker. This detection approach can be a faster, less-invasive, and less laborious alternative to the currently employed analysis approaches. The proposed approach is based on the reported dysregulation of certain microRNA biomarker as a response to hypoxia [2], [5], [10].

In short, the project is focused in answering the following central research question.

How can genosensor be applied to detect microRNA hypoxia biomarkers for clinical diagnosis purpose?

The central research question can be dissected into the following sub-questions, focusing on different pivotal aspects of the outcome.

- What phenomenon underlies reliable signalling for microRNA genosensor?
- What is sufficient level of sensitivity for such genosensor, and how can it be reached?

Chapter 2
Background

Overview

This chapter summarizes background information regarding biomarker as the aim of detection. The definition, applicability, and merit of microRNA biomarkers are presented.

Cancer Biomarkers

Biomarkers (also named as molecular markers or signature molecules) are defined as biological molecules that are also a signature of a certain process/condition or disease [11]. In case of cancers, their level should predict the incidence of cancer. Cancer biomarker molecules can assume different roles in the cancer pathogenesis; they can also take form of different molecules. There are DNA biomarkers, RNA biomarkers, protein biomarkers, or glycol biomarkers [12]. Cancer biomarkers that are relevant in this project are reviewed briefly in the following part.

Nucleic Acids

Nucleic acids are essential biopolymers found in all forms of life. There are two types of nucleic acids, ribonucleic (RNA) and deoxyribonucleic (DNA) acid, respectively. They hold important functions in encoding, transmitting, and expressing genetic information responsible for the development and functioning of living organisms [13]. They function in a flow named as the central dogma of molecular biology [14]: DNA segments are transcribed into strands of messenger RNA (mRNA), and in ribosome, these strands are translated into protein.

DNA and RNA have strong chemical resemblances. Both are structured from monomers called nucleotides [15]. Nucleotides are composed of a common phosphate and sugar group, with a differentiating nitrogenous base. The bases adenine (A), guanine (G), and cytosine (C) are found in both DNA and RNA. Organic base thymine (T) can be found only in DNA, and uracil (U) only in RNA. These bases form complementary pairings through hydrogen bonds, where adenine binds with thymine in DNA, or uracil in RNA; and cytosine with guanine. Through this bonding two complementary polynucleotide strands hybridize with each other. [14]–[16] The structure of nucleotides and bonding between them are illustrated in figure 2.1.A. Cytosine-guanine bonding is stronger than that of adenine-thymine/adenine-uracil, caused different number of hydrogen bonds involved in the two pair.

The two hybridized strands coil round the same axis in a right-handed fashion, constructing a double-helix structure with diameter of 2 nm. In this hybridized duplex, the sugar-phosphate units create a negatively charged backbone on the outside of the duplex, with the nitrogenous bases in the inside, stacked above one another with space of 3.4 Å between each stack [15], [16]. The structure is given in figure 2.1.B for clarity.

The strong hydrogen bonds between the bases, along with π-stacking (attractive, non-covalent interaction between aromatic rings), keep the duplex stable [17]. However, phosphate residues on the backbones are negatively charged [16], making the backbones to repel each other. Duplex stability increases with the increase of salt contents in the solution as they screen the repulsive negative charges. Deviation of neutral pH and increase of temperature also destabilize the duplex structure [16]. The duplex stability is conventionally expressed by its 'melting temperature'. It is a temperature at which, under the given conditions, half of the duplexes is denatured to single strands. This can be determined experimentally based on the absorbance of 260nm ultraviolet light. Single strand polynucleotides have higher absorbance at this wavelength due to the lack of stacked bases. [16] Therefore, the melting temperature of a duplex can be determined from the temperature-absorbance plot.
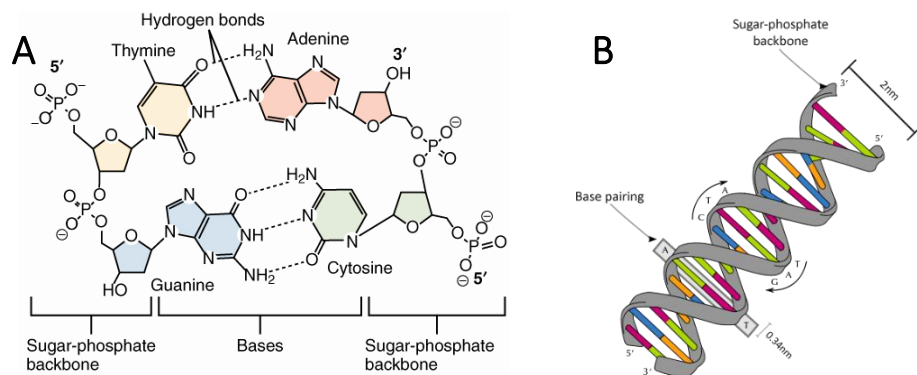
Figure 2.1. (A) Nucleotides structure and hydrogen bond between them (B) DNA structure and dimensions illustration

In 1993, the conductive properties of DNA duplex were demonstrated [18]. Photo-induced electron transfer observed between two intercalated metal on the opposite ends of a 15-base pair DNA duplex showed that be nitrogenous base pairs can facilitate long range charge transport. Since then, this property has been studied extensively, as it introduced many potential applications [19]–[21]. The most interesting application for this project is the application for detecting DNA damage and repair [21], [22].

microRNA as Cancer Biomarker

The human genome is currently approximated to contain around 20,000 genes, where a mere 1.5% codes protein. The rest of the non-protein-coding genes were first regarded to be of no use [23]. However, it was found that a high percentage of these genes are also translated into RNA, the more functional polynucleotides, suggesting that they serve certain functions. This eventually led to the discovery of a class of functional non-protein-coding ribonucleic acids, to be later named as microRNAs [24].

MicroRNAs (miRNAs) are endogenous RNAs with length of 18-22 nucleotides found in most eukaryotes. It has now become evident that miRNAs play an essential role in regulating gene expressions at post-transcriptional level. With more than 900 distinct miRNAs in human genome, they account for up to 5% of the human genes, regulating more than 30% of the protein-coding genes [25]–[27].

miRNAs perform gene expression regulation through several modes of action. Despite the difference, generally miRNAs have gene-silencing effect. A single miRNA can regulate many different mRNAs (up to hundreds), and the expression of one mRNA can be regulated by multiple miRNAs. This highlights the substantial influence of miRNAs in regulating gene expression. While individually miRNAs have minimum repressing effect, jointly miRNAs regulate almost all cellular pathways [28].

Dysregulation of miRNAs has been associated with various human diseases [29]. One of most studied ones its role in human cancer. In case of cancers, genes coding for regulation of cell's life cycle are of high relevance. One type of such genes is the oncogenic miRNA genes; as they override apoptosis, making cells to survive and proliferate instead. Up-regulation of such miRNAs induces cancerous growth. Conversely, tumour suppressing miRNA genes can also play a role. Its under-expression also leads to uncontrolled cancerous growth [6]. The proposed approach is based on the dysregulation of certain microRNAs as a response to hypoxia in cancers.

Despite some detection challenges, miRNAs have proven its merit as biomarker. Circulating endogenous miRNAs are proven to have high stability. Its level is not affected by digestion with Ribonuclease or extreme pHs [30]. This contrasts with exogenous miRNAs that are rapidly degraded in serum. Endogenous miRNAs gain their stability by forming complexes with proteins [31] or by being encapsulated in particles [32]. Circulating miRNA biomarkers are present in minute amount, estimated between 200 aM to 20 pM concentration level [33].

Along with the numerous pathways altered by hypoxia [34], many microRNAs have also been studied to be subsequently dysregulated [35]–[37]. The project did not study the pathway regulation of a specific microRNA. Instead, it aimed at a more general sensing method applicable in detecting microRNA biomarkers.

Chapter 3
Situational and Theoretical Analysis

Overview

This chapter describes and reviews range of biosensors developed in the past years. Advances in the relevant fields are presented and discussed in relation to the project's aim.

Genosensors

Biosensors are sensors using biological substrate in targeting (bio) molecules. Most minimally, biosensors entail a biological recognition layer (bioreceptor) and a transducer. Bioreceptor selectively reacts/interacts with the analyte. This reaction or interaction provides a signalling that can be transduced into electrical signal, performed by the suitable transducer. Various setups of biosensors have been developed in the last decades. Different bioreceptors have been used, such as DNA [38], antibody [39], enzyme [40], [41], etc. As well as numerous transduction methods, such as optical [42], piezoelectric [43], and electrochemical [44]–[46].

Traditionally, nucleic acid detection and analysis were dominated by polymerase chain reaction (PCR) based methods [47], [48]. PCR analysis relies on synthesizing copies of DNA of interest. Through temperature modulation, polymerase enzymes can be employed to create DNA chains of a specific gene, specified by attachment of specifically designed primers to the original DNA strands. Different enzymes can be employed to create RNA strands instead, or to create DNA strands from its RNA counterpart, such technique is called reverse-transcription PCR. The produced DNA can then be isolated and analysed. Mature miRNAs, however, are very small in size that they cannot be assayed by reverse-transcription PCR [49], the most powerful conventional RNA quantitative assay [50]. miRNAs have, on the other hand, very much similar size/length to probes used in hybridization-/genosensors, making this a suitable detection strategy for miRNAs.

Genosensor is a type of biosensors, predominantly used to quantify the expression of a gene of interest. Signalling of a genosensor depends on hybridization between DNA target strands and the complementary DNA probes immobilized on solid surface. Base-pairing provides excellent recognition properties since it is selective and robust [45]. This biosensor field has grown significantly with the growing interest of genetic diagnostics, especially after the mapping of the human genome [51], [52]. Genetic diagnostics brought a new angle of timely disease diagnostics, thus improving disease prognosis and allowing genetic therapeutic approach [53]. Nowadays, one of the most sough-after applications would be the point-of-care diagnostics [54], [55].

Optical Genosensors

Optical biosensors make use of optical transducers to signal the selective reaction between bioreceptor and the sample analyte. Signalling sources from the difference in optical character before and after reaction; in genosensors, before and after hybridization. Several methods are available, namely using fluorescence [42], [56]–[58], surface plasmon resonance (SPR) [59], chemiluminescence [60]–[62], etc.

Early fluorescence approach required target labelling step [57], [63], therefore they are not of high interest for this project. Most interesting genosensors were developed using the molecular beacon approach: nucleic acid strand with self-complementary ends, forming thus a stem-loop structure. For molecular beacon genosensing, one end of the probe strand is modified with a fluorophore (chemical compound that absorbs light of certain wavelength and re-emits light at another wavelength), while the other end is modified with a quencher (another compound that absorbs re-emitted energy and dissipates it as heat) [42]. In absence of target DNA, probes are in the stem-

loop conformation. When the fluorophore is excited, it emits light at its emission wavelength. However, the stem-loop conformation brings the fluorophore in close proximity with the quencher. The emitted light is then quenched. Contrariwise, in presence of target DNA, the probes hybridize and forms the more thermodynamically stable duplex conformation. The fluorophore is then distanced from the quencher, allowing it to fluoresce upon hybridization [42]. This fluorescence (at fluorophore's emission wavelength) is monitored by a photodetector, outputting information about hybridization rate, and thus level of target DNA. Single-nucleotide polymorphism selectivity level has been reported using such setup [64], [65]. It was achieved by sensing within temperature window at which the less-stable single-base mismatched duplex is dissociated but fully matched duplex is stably hybridized.
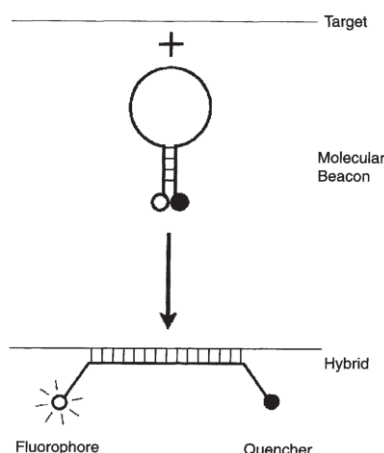
Figure 3.1. Optical detection scheme using molecular beacon (taken from [42]*).*

Another popular optical label-free optical approach is the SPR. SPR requires a demanding setup where a single wavelength light is shone on a thin (gold) platform, which reflects the light unto a detector [66], as pictured in figure 3.2. On the other side of the platform, bioreceptor layer is formed. This layer is placed close enough with the platform, allowing it to resonate with light's evanescent wave. The SPR biosensing then sources from the change in refractive index close to the surface caused by adsorption of analyte. This alters the angle of minimum reflective intensity. This angle shift is proportional to the mass of the analyte adsorped on the bioreceptor layer [59].

In case of genosensors, DNA probes are immobilized to recruit the target strands unto the surface. Hybridization rate with target strands causes proportional shift of the SPR angle. This makes SPR, apart from label-free, also a wash-free and real-time system.
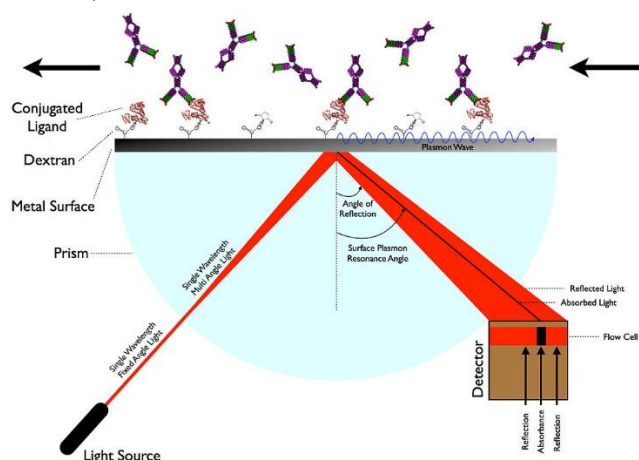
Figure 3.2. Principle of surface plasmon resonance biosensing. Image is taken from [67]*.*

Piezoelectric Genosensors

Piezoelectric material is certain type of material that deforms in application of electric field. Such characteristics are exploited to create a mass-sensitive sensor [43], [68]. Piezoelectric genosensors commonly use quartz crystal microbalance (QCM) as the piezoelectric material. The quartz' resonant frequency depends on the total oscillating mass. Therefore it increases when extra material is deposited on its surface. In genosensors, probes are immobilized on top of the crystal. Hybridization with target strands add mass to the material. The shift in resonant frequency is then directly proportional to the amount of mass of hybridized target strands [68], [69]. Ultrasensitive label-free, reusable genosensors have been reported with using this system [70], [71]; however, at the expense of complicated setup and expensive equipment.

Electrochemical Genosensors

Electrochemistry is a branch of chemistry concerned with the interrelation of electrical and chemical effects. It studies chemical changes caused by the application of an electric charge and the production of electrical energy by chemical reaction [72]. The branch comprises a very wide spectrum of use and applications. However, analytical use will be reviewed in this document.

Analytical electrochemistry makes use of electrochemical processes to detect or quantify a species of interest [73]. Electrochemical processes are controlled and isolated in such a way that a measurable electrical process is quantitatively related to the concentration of the analyte in the sample. To achieve so, situation on the electrode where reaction of interest occurs has to be isolated.

Electrochemical genosensors directly outputs measurable electrical signal. Therefore unlike optical- or mass-readout setup, electrochemical genosensors do not need complicated transducers. This makes electrochemical genosensors inexpensive with very promising possibility of miniaturization and automation. Electrochemical genosensors have also been reported to be selective and robust enough to analyse complex biological samples in minute amount [74], [75]. Electrochemical readout is also undiscerning of high samples turbidity, as it is a challenge for optical readout sensors [54]. All in all, electrochemical genosensors offer ideal characteristics for an inexpensive, fast, and simple point-of-care diagnostic setup.

Advances in Electrochemical Genosensors

Recent years have seen a lot of works in the field of electrochemical genosensors. The first strategies exploited the inherent electroactivity of the DNA bases by directly oxidizing immobilized DNA strands [76]. Most activity comes from the oxidation of the guanine bases, due to its low oxidation potentials [77]. The oxidation signal then reflects the amount of guanine available for oxidation at the surface of the electrode. Another study [78], [79] showed that signal can be improved through electrocatalytic amplification by introducing metal complexes.

Though this approach requires no modification and is very simple, it suffers from a number of shortcomings. Firstly, since the probe strands also contain guanine residues, they also undergo oxidation. Signalling can be improved by substituting the guanine bases in the probe with inosine, a nucleoside that binds with cytosine (thus preserving selectivity) but with a much higher oxidation potential, allowing guanine oxidation signal to refer to hybridization. The need of special modification, however, downplayed the simplicity of the setup. Oxidation also damages DNA [80]. It is an undesirable trait for genosensor, for it would be limited in durability and lifetime.

Later detection schemes took another approach by using an exogenous species to undergo redox instead of the DNA. Different moieties have been explored for this purpose, from redox enzyme until nanoparticles. Formerly, this redox moiety is modified unto the target DNA strands [81], adding an undesirable laborious step in detection. Popular improvement of the system include a sandwich assay, achieved by attaching a second synthetic sequence to the overhanging bases (bases that are not hybridized) of the captured target strands, as illustrated in figure 3.3.
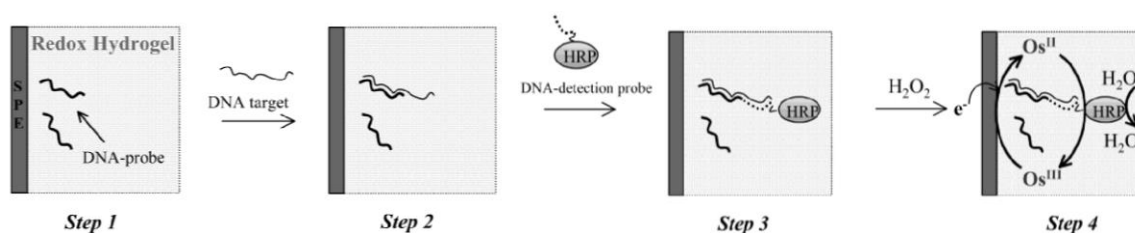
Figure 3.3. Steps of the sandwich-type assay: (1) Oligonucleotide probes are deposited on the electrode; (2) the capture probe and the target are hybridized; (3) the electrode-bound target and the labelled oligonucleotide are hybridized, the labels are in electrical contact with the redox polymer; and (4) the electrocatalytic reduction current of H_2O_2 to water is measured. (taken from [82])

Sandwich assay does eliminate the need to label/modify the analyte. Many variants of electrochemical sandwich assay detection schemes have been demonstrated to achieve excellent sensitivities. Sensor using colloidal gold nanoparticles in sandwich assay format was reported to achieve detection limit as low as 0.8 femtomoles [83].

Application of sandwich assay in miRNA detection has not been studied too extensively, since the small size of miRNAs does not usually allow numerous overhanging bases to work with. Some studies have shown similar ideas for miRNA detection, by using overhanging probes sequences instead. A study [84] demonstrated that a stem-looped capture probes with two complementary regions, one for (synthetic) detection probe and another for the target strands, can achieve a miRNA detection limit of sub-femtomoles level.

Redox moieties that bind intrinsically with DNA duplex have also gained a lot of attention for they do not require any labelling modification. State of the art genosensing uses such moiety in DNA-mediated charge transport to bring selectivity up to single nucleotide polymorphism level. Barton [85] reported a system using probe with intercalating redox tethered on its top. When target DNA hybridizes with the probe, the redox active species intercalates with the duplex. Charge will be transported from the redox species to electrode through the base-stacking of the fully matched duplexes. One unstacked base pair can shut this transport down, resulting in lower redox signal. Thus, this reagentless setup can discriminate single nucleotide polymorphism undiscerning of temperature or destabilization of mismatches.

Another study [86] demonstrated the use of freely diffusing redox-labelled peptide nucleic acid (PNA) probes. PNAs are engineered polymer, designed very similarly to DNA, but without the negatively-charged phosphate groups on its backbone [87]. This eliminates the cumbersome immobilization process. Detection was based on repulsion between negatively charged electrode surface and the negatively charged DNA (target) backbone. In absence of the target strands, the non-charged PNA probes diffuses freely, bringing redox active label to-and-fro from the electrode surface. In presence of target strands, hybridized duplex are repelled from the electrode surface, preventing the redox label to reach and thus react with the electrode.

Reagentless setups have also proven some merit in the field of electrochemical genosensors. Reagentless sensors allow measurement in homogeneous environment, without freely diffusing mediators [88]. This improves practicality, sample conservation, and even perhaps, in vivo measurements. The simplest, and grown to be very popular, of such setups was proposed by Fan and co-workers [44]. The designed probe is very much similar to the optical molecular beacon approach [42], only with a redox species covalently attached to one end. When these probes are immobilized on the electrode, redox label is placed in proximity to the electrode, allowing efficient electron transfer. Introduction of complementary target strands, probes unravel and distance the redox label from the electrode. Electron transfer will be then inhibited; decrease of redox current is related of the concentration of target strands. The group reported detection on picomolar level with such setup.

Electrochemical Cell and Measurement

Electroanalysis requires a setup to attain a well-defined situation in order to establish a quantitative relationship between certain electrical quantity and the amount of analyte present [73]. Such is arranged in

electrolytic cells, where reactions are effected by application of external voltage. Electrolytic cells comprise of electrolyte and electrodes. Electrolyte is a solution in which ions are dissolved. Electrodes are electrical conductors used to make contact with non-metallic part of the circuit, in this case the electrolyte.

Most typically, cell reaction of interest takes place on one electrode. This electrode, termed as 'working electrode', is coupled with a non-polarizable electrode called the 'reference electrode' thus completing a closed circuit. All measurements are measured against the potential of reference electrodes, therefore they need to have a known, unchanging potential. In two-electrode cells, current flows through the reference electrode, which disturbs the potential of the reference electrode. Therefore for sensitive analytical setup, a three-electrode setup is needed. [72]

Three-electrode cells employ a third electrode, named as 'counter electrode' or 'auxiliary electrode'. Current will flow between the working and counter electrode, instead of the reference electrode. Counter electrodes should not undergo redox reaction by electrolysis that might produce interfering substances, so they are typically made out of inert materials. This way, voltage can be applied and measured accurately relative to the unchanging reference electrode. [72] Choices of used electrodes/electrodes material depend on specific application.

An electronic instrument named potentiostat is used to drive and measure the cell reaction. Different experimental setup can be realized with a potentiostat and electrolytic cell. Analytical chemistry makes use of a number of different techniques, e.g. potentiometry [89], voltammetry [90], [91], electrochemical impedance spectroscopy (EIS) [92], etc. Potentiometry is a passive measurement system. Though practical, it is very limited in its application. Potentiometric construction is only mostly used for reference electrodes. EIS can be a powerful tool in analytical chemistry, as it can provide different information of complex systems. However, it is still rather new in development, and require a more demanding equipment.

Voltammetry techniques are very widely used for its versatility and sensitivity. Voltammetry is a controlled-potential technique, which measures the resulting current. The potentiostat applies voltage across the working and counter electrode, and while the potential on the working electrode is maintained according to certain pattern (fed by the function generator). Working electrode potential is contrasted against the reference electrode, and fed back to the potentiostat through a high-impedance feedback loop. Since potential and current are directly related to each other, maintaining/modulation of potential will cause in (unique) modulation of the current. This current is then monitored for it corresponds to the amount of electrons needed sustain support electrochemical processes at the given potential. [72] This scheme is presented in figure 3.4 below.
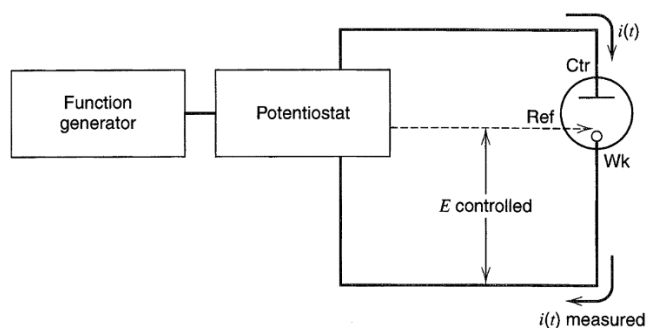
Figure 3.4. Schematic representation of potentiostat (taken from [72]*)*

Two different sources of current contribute the read-out of the system. First is the capacitive/non-Faradaic current. Ions in the solutions will either be attracted or repelled by the potential applied to the electrode. This creates an uneven charge distribution, called the double-layer, which induces the displacement current. This current is generally small and unchanging over limited potential ranges; it is usually termed as a background current. Secondly, the Faradaic current, originating from the electrochemical transformation of electroactive species and thus transfer of electrode across the electrode-electrolyte interface.

By applying negative potentials to the working electrode, the energy of the electrons is elevated. If the energy is high enough, they can flow from the electrode into the vacant electronic state of the electronic species. This current is named reduction current. Contrariwise, positive potentials will lower the electrode's electron energy. At low enough energy, electrons in the electrolyte find a more favourable energy in the electrode and flow there. This results in cathodic current. At which potentials these processes occur is unique to the substances involved and their standard potentials (E^0).

From voltammetry techniques, information from the measured current is usually plotted either against time or potential (or both). In potential step techniques (e.g. chronoamperometry), where potential is modulated from one to another one step-wise manner, current is often times plotted against time. However, this technique only interrogates electrochemical behaviour of the system at one given potential. Numerous experiments is necessary to attain complete electrochemical behaviour of the system. Therefore, sweeping techniques are more commonly used, where potential is swept/varied linearly with time. The current is recorded as a function of the applied potential and plotted the i-E plot or a voltammogram. There are mainly two different conventions used in presenting a voltammogram. In this document, the IUPAC convention is used in compliance with the international standard. The noting of this convention is given in figure 3.5.
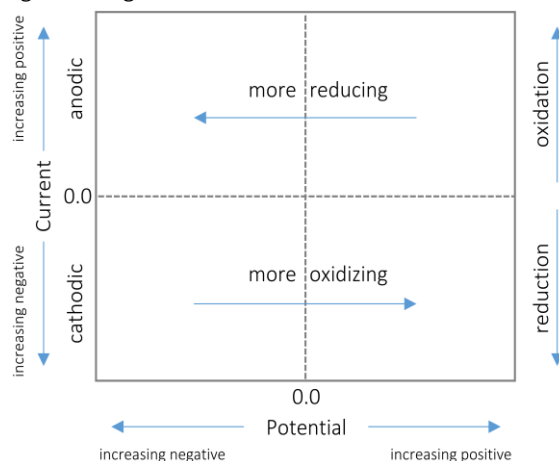
Figure 3.5. IUPAC convention of voltammograms

By differing the applied potential waveform and current measurement strategy, different techniques of voltammetry are available, such as the cyclic voltammetry, differential pulse voltammetry, square wave voltammetry, etc. Each technique has their own advantages, provides different information, and therefore can be used for many different analytical purposes. For our purpose, we first need sensitive technique to obtain information of an unknown system.

One useful method for this purpose is cyclic voltammetry (CV). A triangular waveform of potential is applied in CVs. The potential is swept linearly forward and back between two predetermined potentials (named potential window). This method is very useful in initial characterization of complicated electrochemical processes taking place at the electrode-solution interface [72].

A typical applied waveform in CV is given in figure 3.6.a. When such waveform is applied to an electrolytic cell in presence of a redox active species, voltammogram as such in figure 3.6.b is obtained. The redox species undergo the following reaction.

$$OX + ne^- \rightarrow RED \qquad\qquad (3.1)$$

Where OX is the oxidized form of the species, n represents the stoichiometric number of electrons involved in the process, and RED represents the reduced form of the species. For illustration purpose, the species' E^0 is set to be -209 mV.

Initially, insufficient energy is present to drive any electrochemical reaction, so only non-Faradaic current is observed. As the voltage becomes increasingly negative (approaching species' E^0), species starts to undergo reduction. This decreases the surface concentration of OX, followed by more OX diffusing from bulk to surface. More and more OX undergoes reduction, resulting in increasing reduction current. As voltage is swept past E^0, reduction is very rapid that surface concentration of OX reaches 0, ensuing maximum diffusion rate. Since the potential is still further swept, but mass transfer is already at its maximum rate, depletion takes place. The reduction is then limited by availability of substance on the electrode surface, this can be observed in the drop of reduction current, making the reduction curve to have its 'peak' shape. Once the potential sweep is reversed, similar mechanism takes place for the oxidation process of the RED.
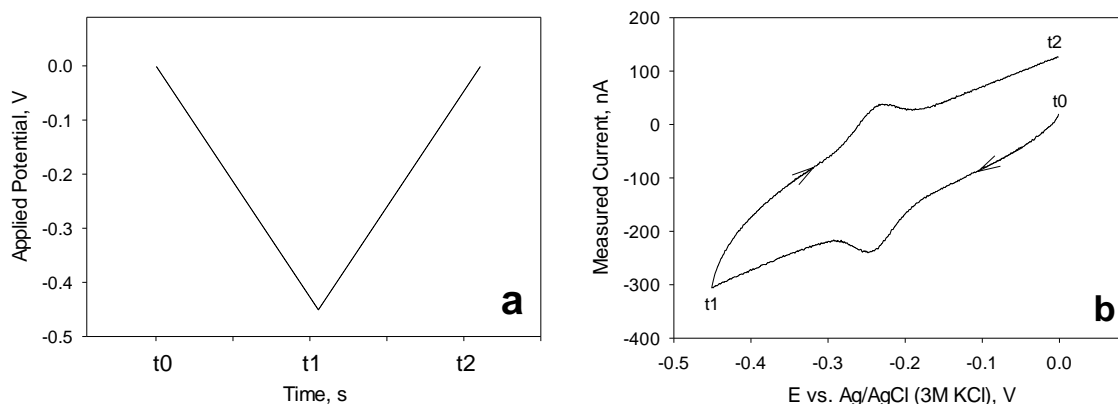
Figure 3.6. (a) Typical applied waveform of CV (b) Example of cyclic voltammogram, time-point correlated with (a)

Another type of voltammetry of interest is the differential pulse voltammetry (DPV). A waveform of a pulse of constant amplitude, modulated on top of a staircase (illustrated in figure 3.7.a), is applied. Current is sample before and after application of modulation pulse. Taking the difference between the two measurements lessens the influence of background current, resulting in a more sensitive technique than the normal sweeping techniques. On the other hand, DPV results in a simplified voltammogram (illustrated in figure 3.7.b) when compared to CV's. Thus less (qualitative) information is obtained, while a relatively more complicated measurement protocol is necessary.
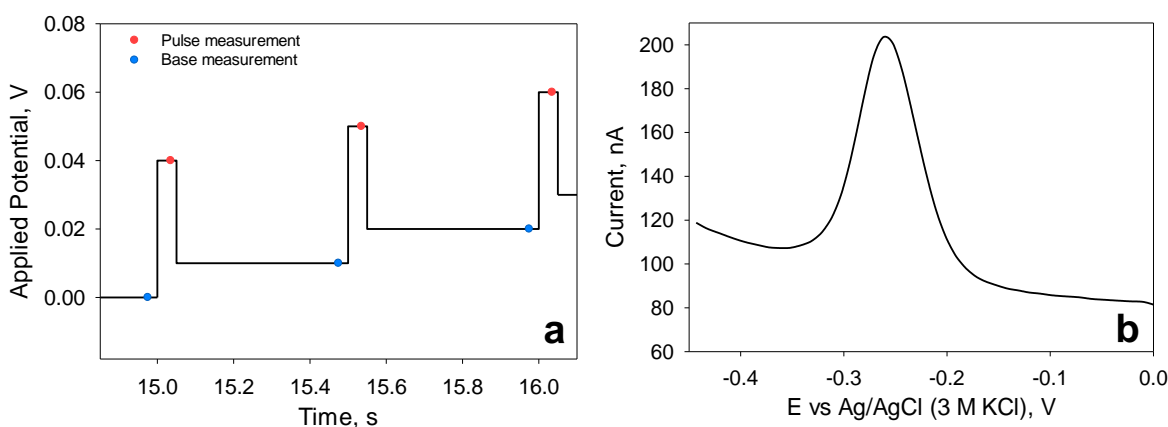
Figure 3.7. (a) Typical applied waveform of DPV (b) Example of differential pulse voltammogram

Hypothesis

The above information postulates that genosensors for microRNA detection can be realized, and that electrochemical detection offers apt features for clinical application. Gene clinical diagnostics do not require

20

massive data accumulation/multiplexing. Instead, reliability and generality of sensor application are of great importance. Therefore this project strives first for sensor's reliability. Optimum sensitivity, practicality, and speed of assay are also addressed to some extent.

Chapter 4
Conceptual Model

Overview

So far, the motivation and aim of the project have been made clear. Relevant advances in the field have also been presented, along with the hypothesis statement. This chapter explores in more detail how electrochemical genosensor for microRNA can potentially be realized for our objective. Choices regarding components/building blocks of the genosensing and processes involved in the sensing are discussed separately, leading to the envisaged genosensor.

Transduction Method

Different biosensor transduction methods were already given briefly in the previous chapter. The mentioned methods are contrasted in table 4.1, especially in their applicability for genosensing. As mentioned already, electrochemical surpasses other reviewed common readout methods in applicability for point-of-care and/or clinical application. There are challenges in reaching an ultrasensitive electrochemical genosensor, however it offers the most robust, cheap, and versatile readout method for our purpose.

Transduction Method	Pros	Cons
Optical	Can achieve high sensitivity; inherent absorbance trait of DNA base-stack; can potentially operate with minute sample amounts; SPR is real-time.	Cumbersome and expensive equipment; sample turbidity can be a concern (except for SPR); fluorophores are not photostable and have non-uniform rate of photobleaching [45]; SPR might require amplification [59].
Piezoelectric	Can achieve high sensitivity; label-free; real-time.	Cumbersome and expensive equipment; challenging fabrication [43]; selectivity challenge operating in rich matrices; temperature sensitivity.
Electrochemical	Low-power; outputs directly electronic signal; simple equipment; promising for miniaturization and automation; can operate with minute sample; stable redox active labels.	Sensitivity might be a challenge; operation in rich matrices risks interference from other (non-specific) electroactive species.

Table 4.1. Comparison table of genosensing transduction methods

A number of different electrochemical interrogation methods have also been briefly presented in the previous chapter. Table 4.2 recaps the advantages and disadvantages of the methods. Practically, both voltammetry and impedance spectroscopy can both be useful methods in the development of genosensor. However, given the available equipment and limited time, the project focused on using voltammetry methods. Voltammetry should also give enough information necessary in the research, and its versatility allowed a lot to explore.

Interrogation Method	Pros	Cons
Potentiometric	Passive measurement.	Not sufficient for self-determining measurement system; limited sensitivity;

		most probably, selective membrane is necessary.
Voltammetry	Versatile; has different interrogation methods; wide applications.	Active measurement, interference of background current.
Impedance spectroscopy	Provides some other information, compared to voltammetry measurements.	Active measurement, demands more complicated equipment; more expensive.

Table 4.2. Comparison table of electroanalysis interrogation methods

Voltammetry's versatility can be seen from the different techniques available. Table 4.3 compares the different techniques. Based on the depicted information, cyclic voltammetry (CV) is very suitable for initial characterization of an unknown system. Resulting cyclic voltammogram reveals a lot of information of system's general response, as well as system's reversibility and kinetics. It is also one of the most used techniques in genosensor research. Therefore a lot of published information can be used as comparison in this research.

For quantification protocols, pulse voltammetry techniques (i.e. differential pulse voltammetry and square wave voltammetry) are preferred for their increased sensitivity, as well as clearer voltammograms. The symmetrical, unambiguous voltammogram allows more accurate data processing for quantification purposes.

Voltammetry Techniques	Pros	Cons
Chronoamperometry	Simple protocol.	Only gives information at one potential against time (E, t plot); substantial measurements needed to obtain wholesome information [72].
Cyclic voltammetry	Characterize system at a range of potentials: outputs (E, i plot) in one measurement; relatively simple protocol; gives information about reversibility, kinetics.	High background current [72], difficulty to use for quantification for the ambiguity of baseline.
Differential potential voltammetry	Moderated background current; highly sensitive for direct evaluation of concentrations; generates clear, symmetric bell-shape voltammogram. [72]	Complicated protocol; simplified voltammogram/current shape.
Square wave voltammetry	Versatile; outputs different diagnostic angles; highly sensitive for direct evaluation of concentrations, generates clear, symmetric bell-shape voltammogram. [72]	Highly dependent on frequency; complicated protocol; no renewal of diffusion layer.

Table 4.3. Comparison table of voltammetry methods

Bioreceptor

It is rather the obvious choice to use nucleic acid polymers as the bioreceptor molecule for genosensors. They offer specificity through the specific base-pairing, and make a robust, easily available probes for hybridizations with target. Apart from DNA, other nucleic acid polymers have been engineered over the years, such as the locked nucleic acid (LNA) and peptide nucleic acid (PNA). LNA has a modified sugar group with an extra bridge [93], enhancing a tighter base stacking [94]. LNA-DNA/RNA duplex have much higher melting temperatures than their natural counterparts because of this organization. PNA is another DNA analogue, but without any backbone charge [87], as already mentioned in the previous chapter. The lack of repulsion between the backbones also results in higher stability of the PNA-DNA/RNA duplex [95]. The engineered nucleic acid polymers offer favourable

characteristics which aid hybridization rate of the genosensors. However, due to their limited availability and higher price, DNA probes will be used in this research. Thermodynamics of DNA probes were first studied to reveal the range of temperature within which the envisaged genosensor can function.

The signalling and selectivity of the genosensors depend vastly on sensor's bioreceptor layer. Many variables need to be adjusted in achieving genosensor for the desired application. Probe design obviously holds a very important role in the functioning and signalling of the bioreceptor layer.

Molecular-beacon/stem-loop probe has been reported to achieve best selective signalling irrespective to read-out techniques [96]. Optical studies [42], [64] revealed that stem-loop probes is uniquely suitable to achieve single-nucleotide polymorphism selectivity level, especially for mutation in the loop part. In electrochemistry read-out, stem-loop probes were reported to have significantly wider optimal frequency range than linear probes genosensors [97]. Table 4.4 summarizes the comparison of all the relevant presented probe configuration.

Probe Structure	Pros	Cons
Linear probes	Unrestricted with self-complementary sequence; predictable immobilization.	Narrower operational.
Stem-loop probes	Wider operational range; elevated selectivity; more predictable single-strand conformation.	More complicated thermodynamics.
Diffusing probes [86]	Immobilization-free; multiplexing possibility is proven.	No regeneration of probes; quantification is not addressed (and potentially limited)

Table 4.4. Comparison table of genosensor probe structures

The choice of probe structure is closely related to the signalling scheme of the genosensor. The schemes visited in the previous chapter are contrasted in table 4.5. For our genosensor purpose, conformational change seems to offer the most benefits, along high promise of success. It is also reflected from the numerous previous studies in different applications of such signalling. This also provides advantage of many works to which the research results can be compared.

Signalling Scheme	Pros	Cons
Conformational change	Reagentless; amendable to multiplexing; suitable for single-nucleotide polymorphism.	Signalling is not as straightforward; probe labelling might be necessary.
DNA bases electrochemistry	Label-free; simple assay.	Limited sensor lifetime, limited multiplexing possibility; high background signals.
Sandwich assay	Potentially label-free; can be multiplexed.	Limited applicability for short microRNAs; probe labelling might be necessary.

Table 4.5. Comparison table of genosensor signaling scheme

Signalling based on stem-loop conformational changes also delivers more reliable results when compared to signalling of linear probes genosensors, where it is solely based on hybridization-induced probe dynamics change [98]. For these reasons, stem-loop probes are used in this project. For operational reasons, such probe should create stable hairpin structure in room temperature (25°C). Conversely, it should not be overly stable either, that hybridization with target is deterred. Such characteristic is amendable through engineering probe's self-complementary sequence [99].

To signal the conformational change, a redox label is modified to the 5' of the probes. Redox probe used is methylene blue (MB), a redox-active species with E^0 of -0.209 V vs Ag/AgCl (3 M KCl) at pH 7 [85], [100]. MB has

grown to be a popular genosensor label for its potential range that is close to those of many biological molecule. Furthermore, such range allows measurement to occur negatively charged electrodes. Repulsion between the surface and DNA/duplex make the strand to be vertically oriented in a more predictable way.

The label is modified unto the 5' terminus through a C_6 linker. This linker is long enough to allow mobility of the label to reach the bulk solution as well as to potentially intercalate into the duplex. However it is not too long that label reaches electrode surface independent of hybridization/conformation of the probe [85]. The probe is modified with thiol on its 3' terminus (also through a C_6 linker) for its reported flexibility. DNA immobilized on its 3' terminus has been reported to have more flexibility than those immobilized on its 5' terminus [101].

Bioreceptor Monolayer

Assembly of Monolayer

In constructing the genosensor, DNA probes need to be attached on electrode's surface where it will recruit target strands to the electrode surface through the specific base-pair interaction. Probes are preferred to be attached on one of its ends, to allow conformational change-induced signalling as well as to ease target strands in reaching these probes [102], [103]. Therefore a site-specific and predictable immobilization strategy is required, to form the monolayer that is stable for the hybridization and measurement time-frame.

Self-assembly methods are often used in constructing a uniform sensing monolayer in a simple, yet predictable way. Since 1983, it has been shown that thiolated compounds form self-assembled monolayer (SAM) on different metals through chemisorption [104]. Thiol-modified DNA probes can be simply incubated on top of the gold electrode, where the strands organize themselves into a stable monolayer on the gold surface. The resulting monolayer has been characterized over the year [105], confirming that it results in strong and robust uniform monolayer, stable for more extended amount of time, more than enough to perform multiple measurements. The self-assembled monolayer is currently the common practice in building genosensors. Other methods (e.g. covalent attachment) would require other specific surface modification, to which access is limited. Therefore no other alternative immobilization approaches are explored for the project.

Nitrogen residues in DNA bases also interact significantly with gold; this may cause DNA to lie down instead of standing upright [106]–[108]. These non-specifically adsorbed DNAs introduce hindrance and might generate signalling that is insensitive to the presence of target strands. As solution, mixed-monolayer can be formed instead. After thiolated-DNA strands are adsorbed, the surface is then exposed to a second thiolated 'backfilling' species/diluent. Mercaptohexanol (MCH) is commonly used as backfilling agent for its insulating property and its suitable length, allowing optimum self-organization [109]. MCH will adsorb on the electrode surface, filling uncovered parts of the surface and remove non-specific, weakly adsorbed DNA strands. This two-steps surface modification (as illustrated in figure 4.1) results in a specific, uniform, and insulated modified surface. Concentration of MCH exposed to the modified surface can also be used as a surface coverage-tuning tool [107].
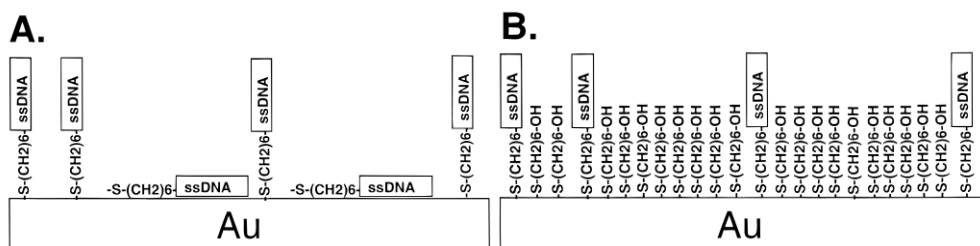
Figure 4.1. Schematic representation of two-steps self-assembly process. (a) First deposition of DNA strands (b) MCH backfills uncovered surface and removes weakly adsorbed DNA strands (taken from [107]*).*

Some variations in the two-steps self-assembly process have been introduced. Firstly, the inversed two-steps method [110], where first the diluent was deposited on the electrode, followed by the probes. Imaging results

suggested that this method resulted in more diluted, but more homogeneous layer of binary monolayer. An optimized one-step modification was also put forward by Doneux, et al [111]. It was suggested that it was possible to deposit both diluent and probes together in one step by carefully adjusting the solution concentration ratio. This method was suggested to result also in more diluted layer of probes, but perhaps more homogeneous. All strategies have been reported to have merit in their applications. Therefore the most suitable procedure was studied experimentally.

Assembly Techniques	Pros	Cons
Conventional two-steps	Widely reported (a lot of examples to study from); well-characterized; can be fine-tuned.	Can result in inhomogeneous layer; more cumbersome protocol.
Inversed two-steps	Result in more evenly distributed probes.	Result in diluted layer; more cumbersome protocol.
Coadsorption	Optimized one-step protocol; result in more evenly distribute probes.	Not yet widely studied.

Table 4.6. Comparison table of mixed monolayer assembly techniques

Surface Coverage

An important variable in the overall performance of the genosensor is the surface coverage of the DNA probes, which describes the density at which the probes are immobilized; usually expressed as Γ in picomole cm^{-2}. Clearly, enough probes should be present to generate adequate signal. However, too dense monolayer will introduce steric hindrance for the target strands and deter hybridization [66]. Furthermore, signalling mechanism can also be vastly affected by surface coverage.

Conveniently, there are means in experimental procedure of fabrication that can tune the fabricated DNA monolayer surface coverage. Probe concentration and incubation time are directly related to the resulting surface coverage [112]. Ionic strength present during SAM formation is also a powerful tool in tampering surface coverage. High ion concentration can screen/neutralize the repulsive negative charges of DNA backbone. With less repulsion between the DNA strands, more packed layer can be formed.

Most of the reported successful conformational genosensors operate at surface coverage below 4 picomole cm^{-2} [44], [113]. This agrees with the work dedicated to study the relationship between surface coverage and hybridization efficiency of hairpin probes [114]. The study revealed that most efficient hybridization (at ~90% efficiency) was achieved at surface coverage between 1-2 picomole cm^{-2}. Therefore as a rule of thumb, surface coverage range of 1-4 picomole cm^{-2} is worth to be studied.

Signalling Mechanism

As discussed earlier, project strives for sensor's reliability. One drawback in using a stem-loop probe is its unattractive signal-OFF reporting [44], [115], where presence of target is inferred from the decrease of signal. Especially when operating in a complex biological matrices, signal-OFF reporting scheme is vulnerable to false-positive outcomes. In rich matrices, many non-specific interactions can compromise or interfere with bioreceptor integrity or desorb the probes altogether, these cases will result also in decreased signal amplitude. Therefore it is preferred that such response is not associated with positive result. Furthermore, from technical point-of-view, signal-OFF can only have operational limit of signal suppression up until 100%. Signal-ON reporting (presence of target analyte is then correlated with increase of signal amplitude), can theoretically have unbounded signal increase.

Recent years have reported numerous works in engineering signal-ON genosensors [116], [117], [113]. One of the simplest approaches in modifying the use of stem-loop probe was suggested by simply using truncated probes [113]. Shorter probes hybridize to form rod-like duplexes that undergo rotational movement governed by diffusion.

In sufficiently diluted surface coverage and with negatively charged surface electrode, this movement can bring redox active species (in this case, methylene blue) tethered on the probes to reach electrode surface.

It is noteworthy that there are other models that might fit application objective. However, this simplest setup holds high promise for success as well as high commercial interest for its (potentially) reagentless, simplistic design. Furthermore, in the framework of the project itself, technical laboratory works will be performed by entirely inexperienced student. Therefore, this simplistic setup is highly favourable over other approaches that might require multi-step hybridizations, etc.

Genosensor Model

Previous parts present envisaged genosensor design part by part. Here, the whole model is summarized and presented.

A stem-loop DNA is used as probe. Its 3' terminus is modified with thiol for immobilization on gold surface (through thiol-gold self-assembly), and its 5' terminus is modified with methylene blue redox label through C_6 linker. In absence of target strands, probe will be conformed in stem-loop structure, confining redox label unto electrode surface.

In presence of complementary strands, probe will hybridize to form a rigid rod-like duplex conformation. Such rigid duplex should undergo rotational movement, displacing the redox label to and from the electrode surface, facilitating redox reaction of probe. Signal-ON response can be calibrated against the amount of complementary strands presence to evaluate genosensor's performance.

Chapter 5
Research Approach

Overview

In answering the research questions, sets of experiments were performed. This chapter recaps and details the experiments done in the course of the project. The experimental setup used is elaborated, followed by the different reasoning/purposes of the different experiments done in the project.

All experiments were done in the facility of Electrochemical Biosensors and Bioelectrocatalysis group at iNano, Aarhus.

Experimental Setup

For the envisaged genosensor, gold disk working electrode (with diameter of 1.5mm) was used, for its favourable characteristic in achieving the self-assembling bioreceptor layer. Platinum electrode with high surface area was used as counter, chosen mostly for convenience. As reference electrode, silver wire coated with a thin layer of silver chloride was used, named as the silver-silver chloride electrode or 'Ag/AgCl'. It is typically enclosed in potassium chloride solution. For the experiments, Ag/AgCl reference electrode (purchased from Sigma-Aldrich, Germany) kept in 3 M potassium chloride was used. For this constant make up, its potential was fixed at 210 mV, compared to normal hydrogen potential (NHE) [118], [119]. Ag/AgCl reference was used for its stability, availability/practicality, and non-toxicity.

Electrochemical cell, with electrolyte volume of ~3mL, was used. Taking into account the small gold electrode size when compared to the amount of electrolyte, this cell size was still regarded as a small A/V (area/volume) system, where reaction at the electrode surface was regarded as not to alter cell's bulk concentration. The electrodes (especially the working and reference electrodes) were put at a fixed distance of around 1 cm for each experiment, to achieve moderate and comparable Ohmic drop between measurements.

Metrohm potentiostat (µAutolabIII/FRA2) ran the experiments, with protocols programmed in the NOVA 1.8 software.

Characterization of Gold Electrodes

The conceptualized sensing signalling originates from conformational changes introduced by hybridization with complementary strands. In order to achieve efficient and reproducible signalling, it was important to have a clean smooth surface of the gold electrode. Therefore, firstly, a study to characterize gold electrodes was carried out. During this phase, I also learnt to attune to the preparation of gold electrodes, as well as practical electroanalytical chemistry in general.

Immobilization Strategies

Different immobilization strategies were also visited briefly in the course of the project. The strategies named and elaborated in table 4.6 were studied experimentally. Process and results are included in appendix B.2. Based on the outcome of the study, conventional two-steps modification method came to be most resource-efficient method, with relatively consistent results. Results were only reflected from electrochemical interrogation methods, due to lack of access to molecular-level imaging equipment. Nonetheless, electrochemical results obtained were consistent with published works [44], [85], suggesting that (mixed) monolayer was formed in the predicted way.

Thermodynamic Study

To accurately observe the envisaged signalling scheme, thermodynamic study was also required. Melting temperature of different foldings/duplexes holds important role in the sensing. Both theoretical and experimental studies of melting temperatures were done. Theoretical study was based on literatures as well as through the normative DINAmelt algorithm [120], [121]. Results of the theoretical study were contrasted against experimental results.

It was also reported that immobilisation on solid surface affects DNA stability. A study [122] suggested that difference in the dielectric constant between immobilized and bulk solution duplexes results in reduction in effective ionic strength. Decrease in ionic strength renders duplexes less stable, therefore have lower melting temperatures. Experiments have observed lowering of Tm of about 5°C [123]. Due to lack of experimental equipment, Tm of immobilized strands were only reasoned based on published literatures.

DNA Experiments

It is normative when suggesting a new detection method or variation to start with experiments using synthetic oligonucleotides. Such experiments are to demonstrate that immobilization and detection method work as expected and is selective of target strands. This research strives to prove the concept first on this level, operating in physiologically relevant buffer condition.

The proven concept was then transferred to the aimed microRNA genosensors. Where the performance was once again evaluated for microRNA affinity. Performance of the modelled system was finally tested in biological serum, simulating biological sample. The more complex matrix might yield different sensing results. This attests sensor's performance in a more representative way for clinical application.

Chapter 6
Characterization of Gold Electrodes

Overview

Prior to each sensor fabrication, gold electrodes needed to be cleaned and characterized. This chapter presents and discusses this process and the characterization of the gold electrodes.

Electrode Preparation Steps

Gold disk electrodes (CH Instruments, Austin, TX; diameter 3 mm) were electrochemically cycled in 0.5 M NaOH between -0.4 and -1.6 V for 10 cycles at 0.05 V s^{-1}, to remove all thiol residues from the electrode surface. Studies carried out in the lab showed that thiols desorbs from gold surface at -1.4 V vs Ag/AgCl (3 M KCl).

To achieve a smooth gold surface [124], the electrodes were mechanically polished [38] on a microcloth pad in 1 μm diamond (Struers, Copenhagen, Denmark) for 2 minutes, followed by another 2 minutes of polishing in 0.1 μM alumina slurries (Struers, Copenhagen, Denmark). The electrodes were washed with Milli-Q water and ultra-sonicated in 1:1 ethanol–water solution for minimum 10 minutes, to remove remaining polishing material [38].

The electrodes were then washed with water and electrochemically polished stepwise in 1 M H_2SO_4 from -0.3 to 1.7 V for 10 cycles at 0.3 V s^{-1} and in 1 M H_2SO_4/10 mM KCl from 0 to 1.7 V for 10 cycles at 0.3 V s^{-1} [38].

Finally, the electrodes were cycled in 0.1 M H_2SO_4 from 0 to 1.7 V for 2 cycles at 0.3 V s^{-1} to determine the electrochemical surface area of the electrode. The clean electrodes were kept in absolute ethanol at 4°C before use.

Characterization of Gold Electrodes

The electrochemical surface area the electrode surface was estimated after the last cycling step by integration of the gold surface oxide reduction peak in 0.1 M H_2SO_4 and by using a conversion factor of 400 μC cm^{-2} [125], the amount of charge needed for one-electron reduction of gold oxide. The electrode surface is considered to be clean, if a reproducible sharp gold oxide reduction peak, with a clear defined 'shoulder' is obtained, as given in figure 6.1.
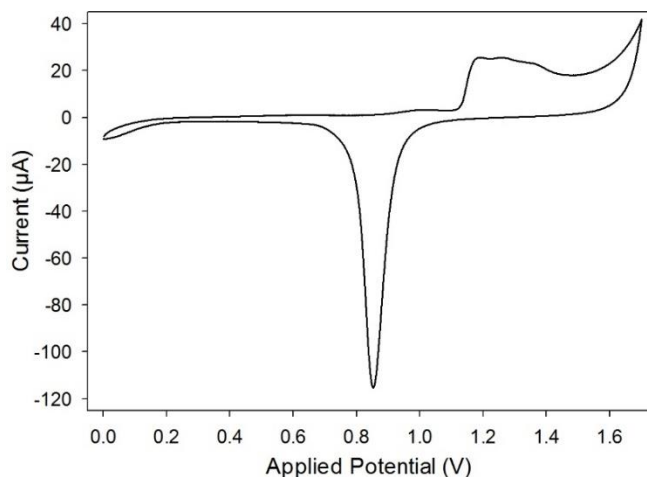
Figure 6.1. Representative CV of clean bare gold electrode in 0.1 M H_2SO_4. Scan rate: 0.3 V s^{-1}.

Impurities on the electrode surface causes a distortion of the voltammogram's gold oxide peak. Figure 6.2 represents a cyclic voltammogram of a gold electrode that was considered to be not clean. Same cleaning steps were repeated for such gold electrodes until a clear defined 'shoulder' is obtained.
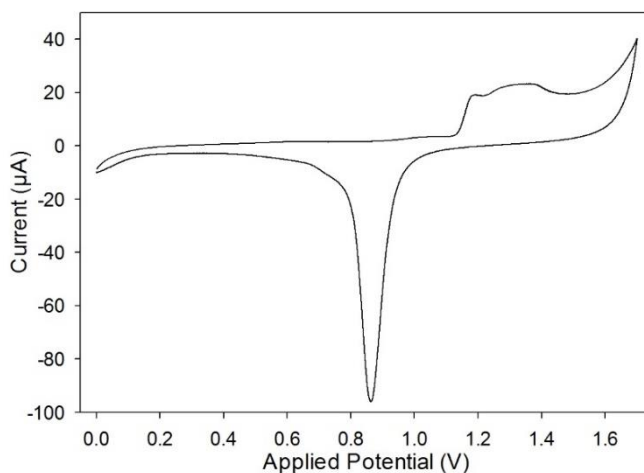
Figure 6.2. Representative CV of not clean gold electrode in 0.1 M H_2SO_4. Scan rate: 0.3 V s^{-1}.

The geometrical surface area of an electrode can be calculated as follows:

$$A = \pi r^2 = \pi \, (0.15 \, cm)^2 = 0.070685 \, cm^2 \qquad (6.1)$$

However, a completely smooth surface cannot be achieved. The roughness of the surface adds to the effective surface area. In a molecular scale process, this difference can introduce a strong inaccuracy to any calculation/determination forward on, e.g. determination of surface coverage. Consequently, the real surface area which contributes to the electrochemical process needs to be determined experimentally.

Roughness factor is defined as the ratio between the electrochemical surface area and the geometrical surface area. Yang, et al [115] studied that folding-based genosensors work comparably well on rough (electrodeposited) gold surface, with roughness factor up to ~7. However, it was also shown that sensors fabricated on electrode surfaces with roughness factor above 4 have less reproducible results. For gold disk electrodes, it is not too challenging to obtain roughness factor below 4. Therefore all experiments will use strictly clean gold disk electrodes with roughness factor below 4.

Electrode Modification with DNA

To fabricate the sensors, clean electrode surface were modified with thiolated DNA strands through self-assembly in a single-point attachment. DNA probe strands, derivatized on its 3' end with disulfide and on its 5' end with methylene blue, were purchased and used as is. Disulfide bonds were reduced with TCEP to obtain accessible thiol ends. TCEP does not contain thiol residues itself, nor does it interfere with thiol adsorption [126]. Therefore TCEP does not need to be removed before cross-linking reactions take place during immobilization.

Solutions containing 10 µM DNA strands in 20 mM phosphate buffer (pH 7) and 0.15 mM NaCl were drop-casted (deposited as a bubble of solution on a surface) on the clean gold disk electrodes. Self-assembly was allowed during 12-16 hours incubation at room temperature. During incubation electrode was covered to prevent evaporation and was protected from light.

Determination of DNA Monolayer Surface Coverage

Big part of the analysis of the genosensors is based on the DNA monolayer surface coverage. Even though all sensors are fabricated under the same protocol, each fabricated sensor is unique to each other. Each electrode has unique gold surface and the monolayer formation is governed by independent gold-thiol interaction. Therefore each fabricated DNA monolayer needs to be studied experimentally.

Surface coverage (Γ) of a monolayer can be defined by the following equation [127], [101].

$$\Gamma = \frac{Q}{nFA}$$

(6.2)

Where Q is the charge passed to the electrode (Coulomb), n is the moles of electrons in the electron-transfer process (for the SAM we will be using n=1), F is Faraday's constant and A is the experimentally determined electrochemical area of the electrode (cm^{-2}). The values of Q can be determined by integration of the methylene blue reduction/oxidation peaks in the cyclic voltammograms of the folded probes, integration is done by software (NOVA 1.8).

Kinetics of Electrode Processes

The signalling of electrochemical genosensors depends also heavily on the kinetics of the processes taking place on the electrode. Kinetic information of a process can be derived from its voltammogram.

As mentioned earlier, there are two different source of currents measured in a voltammetry system. The Faradic process, however, forms the peaks of interest in the voltammogram. This peak is directly correlated to the reaction rate at the electrode surface, which is limited by the concentration of redox species at the electrode surface. Along with the redox reaction, the concentration of the analyte at the electrode surface decreases, and that of redox product increases. Redox reactions occur at a much higher speed than diffusion of these species. Consequently, a 'depletion' area is created, where concentration deviates from the bulk. Figure 6.3 illustrates the concentration gradient of redox species (in this case, $Fe(CN)_6^{3-}$) formed over time when sufficient potential is applied.
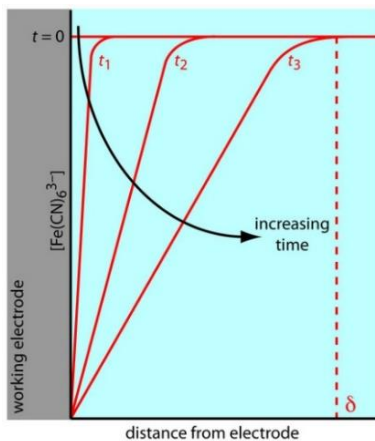
Figure 6.3. Concentration gradients (in red) for $Fe(CN)_6^{3-}$ following the application of a potential that completely reduces it to $Fe(CN)_6^{4-}$. Picture is courtesy of UCDavis ChemWiki [128].

In an unstirred system (no forced convection), the redox reaction is then limited by the diffusion of the analyte from the bulk concentration to the electrode surface. Such system is named a diffusion-limited system. Peak current of such case is governed by the Randle-Sevcik equation given below.

$$I_p = k \ n^{3/2} \ A \ D^{1/2} \ v^{1/2} \ C_b$$

(6.3)

Where the constant k = 2.69 x 10^5; n is the number of moles of electrons transferred per mole of electroactive species (e.g. ferricyanide); A is the area of the electrode in cm^2; D is the diffusion coefficient in $cm^2\ s^{-1}$; υ is the scan rate of the potential in volt s^{-1}; and C_b is the bulk solution concentration in mole L^{-1}. The equation reveals that the peak current intensity is proportional to both the scan rate and bulk concentration. This makes it a good quantitative parameter for analytical purposes.

On the other hand, a system can have absorbed species on its electrode surface. In such case, diffusion does not play a role. The peak current is directly related to the surface concentration of the absorbed species, and is governed by the following equation.

$$I_p = k\ n^2\ vA\Gamma \qquad (6.4)$$

Where the constant k = 9.39 x 10^5; n is the number of moles of electrons transferred per mole of electroactive species; A is the area of the electrode in cm^2; and Γ is the surface coverage of the absorbed species in pmol cm^{-2}.

Experimentally, the kinetic property of a system can be known by studying peak currents as a function of both scan rate and square root of scan rate. Should the peak current be linear to square root of scan rate, it is implied that system is governed by diffusion. A system with linearity between peak current and square root is a surface process, limited by its absorbed redox species.

Gold Electrode Characterization by Diffusion Electrochemistry

The surface of the gold electrode can also be characterized through diffusion electrochemistry in presence of redox mediator, such as ferricyanide ($Fe(CN)_6^{3-}$). Ferricyanide in the solution is reduced to ferrocyanide ($Fe(CN)_6^{4-}$) when reaching the surface of the gold electrode.

Separation between the cathodic and anodic peaks of a system reveals system's reversibility. Reversible systems have the peak separation (ΔE_p) defined as followed.

$$\Delta E_p = \frac{0.059}{n} volts \qquad (6.5)$$

Where n is the number of moles of electrons transferred per mole of electroactive species. Increasing value of ΔE_p suggests irreversibility of the system, caused by some thermodynamic barrier resulting in sufficiently slow electron transfer.
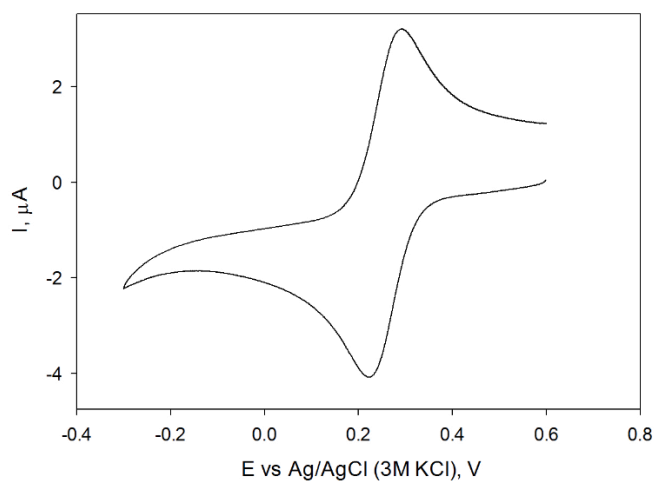
Figure 6.4. Representative cyclic voltammogram of clean bare gold electrode in deaerated solution of 1 mM $K_3Fe(CN)_6$/100 mM KCl. Scan rate: 100 mV s^{-1}.

Figure 6.4 shows the cyclic voltammogram of a clean bare gold electrode in the presence of ferricyanide redox species and KCl as supporting electrolyte. Supporting electrolyte is required to minimize migration of charged redox species in the electric field gradient. Ferricyanide-ferrocyanide is a known reversible redox couple, undergoing one-electron transfer each redox reaction. Therefore ideally, its cathodic and anodic peaks should be separated by 59mV.

From the obtained voltammograms, it was found that the anodic peak of the reaction took place at 0.28501 ± 0.00985 V and the cathodic at 0.21516 ± 0.00914 V. The two are separated by 0.06984 ± 0.00598 V. This value is very close to the theoretical value of peak separation of reversible system. This suggests the system is only limited by diffusion and that the redox couple underwent redox reaction uninhibitedly. This also implies that the electrode surface is free of impurities, since impurities would inhibit electron transfer to some degree.

Chapter 7
Probes and Thermodynamic Study

Overview

This chapter is dedicated in presenting the probes used in the project and the study of their thermodynamics. Conformational change of the probes are governed by their (and the duplexes) thermodynamics, therefore this study was aimed to provide some information of the genosensor's performance.

Two approaches are presented in this chapter: theoretical approximation and experimental approach. Details behind each approach are elaborated separately. The findings are then concluded in the end.

Probes Sequences

There are a number of sequences used in the project. Synthetic DNA sequence of 20 nucleotides was used as a proof for immobilization and detection. Later, similar setup was then applied for the specific microRNA detection. The sequence is chosen based on length,

The hsa-mir-618 and hsa-let-7c microRNA sequences were chosen for this project. Both miRNA sequences are shown to be upregulated by hypoxic environment. miRNA hsa-mir-618 has been reported to be a stable biomarker, with aberrant expression up to 1.5 times more in hypoxia than in normoxia [35]. This specific sequence was also chosen for its similarity with the proven synthetic DNA setup, in terms of length, melting temperature, etc. The second miRNA sequence was used, to observe (roughly) the generality of the setup. Table 1 below sums up the sequences used, complete with the probes modification.

Type	Oligo Name	Sequence (5'-3') and Modification
DNA probe	DNA hsa-mir-618	AttoMB2-CTC TAG AAG GAC AAG TAG AG-Thiol(6-S-S)
DNA probe	DNA hsa-let-7c	AttoMB2-GTA GTT CAC CAT ACA ACC TAC TAC-Thiol(6-S-S)
DNA target	cDNA hsa-mir-618	CTC TAC TTG TCC TTC TAG AG
DNA target	cDNA hsa-let-7c	GTA GTA GGT TGT ATG GTG AAC TAC
RNA target	cRNA hsa-mir-618	AAA CUC UAC UUG UCC UUC UGA GU
RNA target	cRNA hsa-let-7c	UGA GGU AGU AGG UUG UAU GGU U
DNA probe	SyntheticDNA	MB2-GC AGT AAC AAT ACC CAC TGC-Thiol(6-S-S)
DNA target	cSyntheticDNA	GCA GTG GGT ATT GTT ACT GC

Table 7.1. Summary of sequences used. 'c' denotes complementary (target) sequences. Self-complementary region of the probes are underlined.

Melting Temperature Calculation

For each of the sequences, its melting temperature and melting/folding in solution are simulated/estimated theoretically. The process is done using DINAmelt web server. The prediction is based on equilibrium thermodynamic, using the nearest-neighbour model for computation [120], [129]. Nearest-neighbour model suggests that stability of a duplex/folding does not depends solely on the identity of the bases that hybridize (thus the relative content of cytosine and guanine), but also on the sequential composition of the strands [130].

Furthermore, the algorithm in DINAmelt is also regularly updated based on recent research/studies in the field. All in all, it makes the web server very widely used and it is regarded as the most accurate approximation of nucleic acid melting temperatures. The simulated results are tabulated below.

Type	Oligo Name	Melting Temperature in 20 mM PBS (pH 7)/0.150 M NaCl/0.005 M MgCl$_2$
DNA probe	DNA hairpin hsa-mir-618	38.0^{o}C
DNA probe	DNA hairpin hsa-let-7c	37.0^{o}C
DNA duplex	hsa-mir-618 DNA duplex	62.6^{o}C
DNA duplex	hsa-let-7c DNA duplex	66.7^{o}C
RNA duplex	hsa-mir-618 DNA-RNA duplex	60.9^{o}C
RNA duplex	hsa-let-7c DNA-RNA duplex	62.0^{o}C
DNA probe	SyntheticDNA hairpin	55.3^{o}C
DNA duplex	SyntheticDNA duplex	68.4^{o}C

Table 7.2. Melting temperatures of sequences used, hairpin and duplex. Generated by DINAmelt algorithm [129].

Allegedly, the theoretical/simulation calculation showed lower melting temperatures of hairpin folded probes than the probe-target duplexes. Probe-target duplexes are thus the more thermodynamically favourable melting state, which is suitable for the aimed affinity genosensor. All folding/duplexes were also calculated to have sufficiently high melting temperature to allow operation in room temperature (around 25°C). Even when the lower melting temperature of immobilized probes are taken into account [123], the least stable hsa-let-7c hairpin probe would still have a relatively high melting temperature at around 32°C.

The syntheticDNA probe and microRNA probes had different compositions of the self-complementary sequences (table 1, appendix A). This lead to difference in probe melting/folding temperatures, where the microRNA probes had significantly lower melting temperatures than the synthetic DNA probe. Due to the less stable self-complementary sequence, the microRNA probes should have an increased affinity to the complementary strands [99]. It is expected for such probe to achieve lower detection limit than the more stable syntheticDNA probe.

Melting Temperature Measurement

Melting temperature of some duplexes were also determined experimentally. Melting curves were acquired by monitoring absorbance of 260 nm ultraviolet light by the sample as a function of temperature. Experiment was performed by Cary100 Bio UV-visible spectrophotometer. 600 μL of 1.5 μM DNA duplex in 20 mM PBS buffer (pH 7) containing 150 mM NaCl and 5 mM MgCl$_2$ were used as samples for the experiments. Temperature was modulated between 20°C and 80°C in modulation rate of 1°C per minute. To ensure uniformity of states of the probes, three complete heating-cooling transitions were cycled for each sample. The curves from the last transition were used for analysis.

Due to limited access to the experimental equipment, only two samples of the microRNA duplexes could be analysed. The resulting absorbance sigmoidal plots were then normalized, as presented in the following figures. Figure 7.1 presents the normalized absorbance-temperature plot of the hsa-mir-618 fully complementary duplex. 50% of the absorbance, occurred at temperature of 63.52^{o}C; thus defining duplex's melting temperature. This value is very close to the DINAmelt calculated/simulated value of 62.6^{o}C, as given in table 7.2.
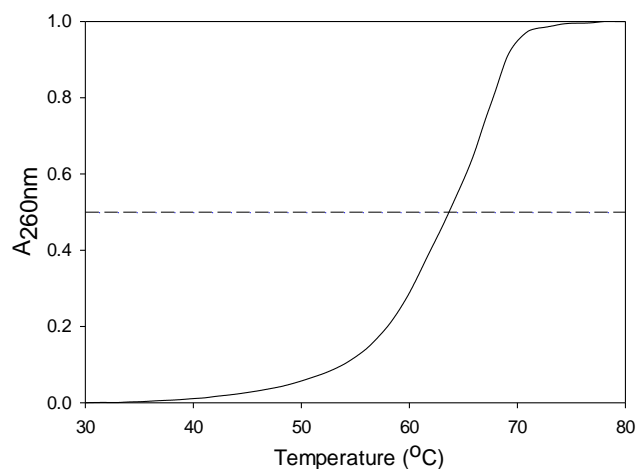
Figure 7.1. Normalized absorbance-temperature plot of hsa-mir-618 DNA duplex in 20 mM PBS (pH 7) containing 150 mM NaCl and 5 mM MgCl₂. 50% absorbance level is also shown for determination of Tm.

Figure 7.2 presents the normalized absorbance-temperature plot of the hsa-let-7c fully complementary duplex. 50% of the absorbance, occurred at temperature of 67.535°C; thus defining duplex's melting temperature. This value is very close to the DINAmelt calculated/simulated value of 66.7°C, as given in table 7.2.
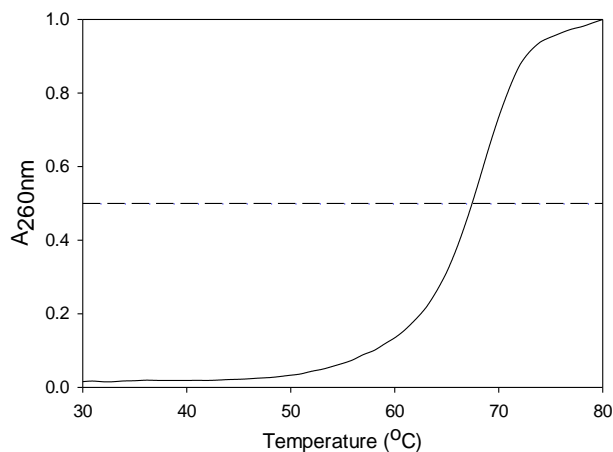
Figure 7.2. Normalized absorbance-temperature plot of hsa-let-7c DNA duplex in 20 mM PBS (pH 7) containing 150 mM NaCl and 5 mM MgCl₂. 50% absorbance level is also shown for determination of Tm.

Conclusion

The theoretical approximation of the melting temperatures of the probe foldings and duplexes revealed that the designed probes possess suitable thermodynamic characteristics to instigate signalling based on conformational change. Experimental data of the duplex melting temperature were in great accordance to the theoretical approximation. Therefore it was safe to assume that the theoretical approximation was accurate enough to use as estimation.

Chapter 8
Samples Analysis

Overview

This chapter presents and discusses the obtained experimental results. Firstly, results obtained from the synthetic DNA analysis are given; followed by the microRNA analysis. Protocol performed in achieving the results is given roughly for each experiment, with the complete protocol included in the appendices.

Synthetic DNA Analysis

Below the results of the synthetic DNA analysis are presented. 20-nucleotide long probe was used, with the sequence given in table 1, under 'syntheticDNA'. The oligonucleotide was modified with methylene blue (containing –COH side group) on its 5' terminus and thiol on its 3' terminus.

The probes were immobilized as single-stranded DNA on clean gold disk electrode surface through self-assembly. Electrodes had electrochemical surface area of 0.080 ± 0.003 cm^2. Self-assembling probes was let for 16 hours and subsequently backfilling with 2 mM mercaptohexanol for 30 minutes. Resulting surface coverage was calculated to be 1.47 ± 0.32 pmol cm^{-2}.

Figure 8.1 shows the cyclic voltammogram of the probe-modified gold electrode. The clear peaks revealed the observable formal potential of the redox label at around -0.23525 ± 0.00448 V, estimated from $E_{1/2} = (E_{red} + E_{ox})/2$ [72]. It was comparable to formal potential of methylene blue in solution. These peaks were not obtained in measurement of electrodes only modified with mercaptohexanol backfilling agent (voltammogram is shown in appendix B.1). The peaks observed in figure 8.1 can then be credited to the redox-active label methylene blue. Based on the comparable formal potential values, tethering also did not significantly alter the electroactivity of methylene blue.

Figure 8.1. Cyclic voltammogram for gold electrode modified with methylene blue-tagged DNA probes in the absence of target DNA in 20 mM PBS (pH 7) with 0.150 mM NaCl. Scan rate: 0.1 V s^{-1}. (inset) Relationship between peak currents and scan rates.

Similar cyclic voltammetry measurements were done at different scan rates, to observe the kinetics at work. Scan rate was varied from 0.05 V s^{-1} until 5 V s^{-1}. Peak currents of the obtained voltammograms were plotted against the corresponding scan rate in the inset o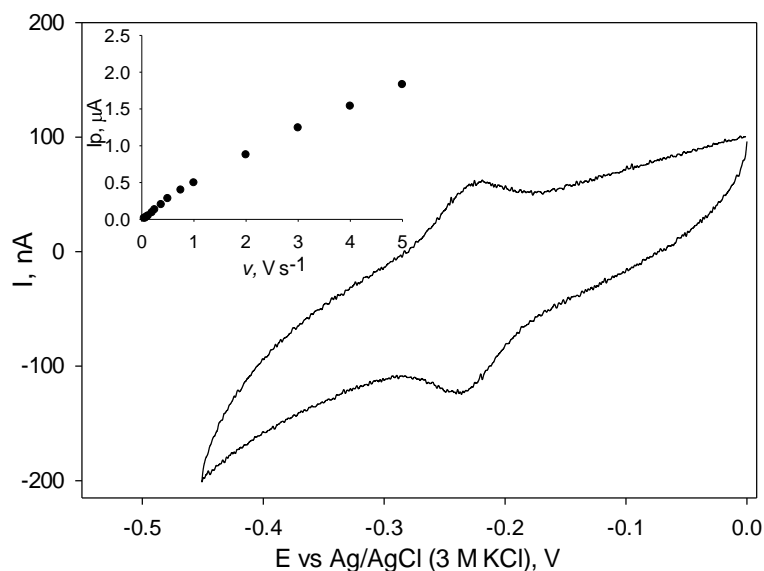f figure 8.1. The linear relationship between the scan rates and peak currents suggested that system was governed by surface process (equation 6.4), by the surface-confined methylene blue. As a contrast, the peak currents were also plotted against the square root of scan rates, as given in appendix B.5, where it showed less correlation.

The fabricated sensors were then studied in presence of target DNA. Sensor response was calibrated in presence of different concentration of target DNA in range of 0.1 nM to 5 μM. Target strands were diluted serially in 20 mM PBS buffer (pH 7) containing 150 mM NaCl and 5 mM MgCl$_2$ to obtain different concentrations. Hybridization was achieved by incubating 10 μL of the target solution on the modified electrodes for 30 minutes. Variability of the sensor was observed from three different electrodes, which were equivalently prepared and measured. Calibration measurement used differential pulse voltammetry (DPV) interrogation method with 40 mV modulation amplitude, 10 mV step potential, and scan rate of 20 mV s^{-1}. Measurement was done in deaerated 20 mM PBS buffer (pH 7) containing 0.15 M NaCl.

The result is presented in figure 8.2 below. Although minimized, capacitive current was still present on DPV measurements. This 'background' current hindered accurate comparison between measurements. Therefore it was corrected by subtracting a polynomial-fitted baseline curve. The baseline curve was fitted manually, done in NOVA software. The corrected voltammograms of the cathodic current are overlaid in the figure 8.2 below.

The presented differential pulse voltammograms showed the expected bell-shaped peak at similar potential with the verified methylene blue peak of the CV. This suggests that DPV also observed the same methylene blue peak. It was observable that the DPV peak current had a much bigger magnitude than CV peaks, making DPV the more sensitive interrogation technique.

The source of signal changes was verified in control experiments. The sensors were challenged with DNA-free buffer as well as non-cognate DNA strands. The process and results of these experiments are presented in appendix B.3.
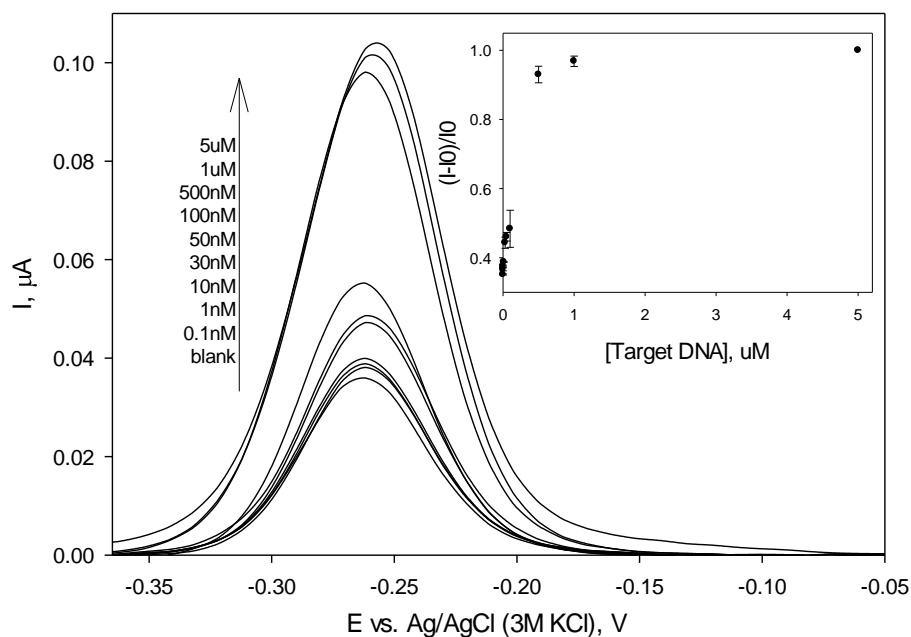

Figure 8.2. Representative baseline corrected differential pulse voltammograms recorded before and after interaction with the complementary target DNA. (inset) Genosensor response across three equivalently prepared electrodes, normalized for the blank, calibrated against DNA concentration.

The sensor showed an increase in DPV peak current with the increase of target DNA present. This signal-ON reporting was consistent with previously reported response of 20-nucleotide long probes [113]. The sensor reacted consistently starting from the presence of 0.1 nM target DNA, suggesting it could detect 1 femtomole of complementary target. Peak current increased linearly with the increase of target DNA concentration up until 100 nM.

At 1.43 pmol cm^{-2} surface coverage, around 150 femtomoles of the DNA should be present on the electrode surface. Theoretically, response saturation is expected at incubation of 10 μL of around 15 nM complementary DNA. Curiously, saturation was observed in presence of around 10.000 femtomoles of target DNA. An unproportioned, sharp increase in the peak current was also observed at incubation of 500 nM target DNA. These suggested that either hybridization yield was considerably low [99], leading to saturation only at 60 fold excess of complementary strands; or the occurrence of secondary phenomenon at sensor's saturation that resulted in amplified DPV signal.

'Background' signal could roughly be obtained again after hybridization by rinsing the electrode surface with Milli-Q water for 40 seconds. Stream of water breaks the hydrogen bonds between the bases, allowing target strand to dehybridize, and probe DNA to conform back to its initial hairpin structure. Comparison of regenerated signal is included in appendix B.4. This also confirmed that the increased of DPV peak current was attributed to the hybridized probes.

Model Evaluation

Overall, the syntheticDNA experiment evidenced a (reusable) signal-ON genosensor based on the conceptualized model, with absolute detection limit of 1 femtomole. The exact signalling mechanism can be inferred from the kinetics study presented in appendix B.5. The diffusion-governed system for the hybridized probes agreed with the conceptualized signalling mechanism put forward in chapter 4.

The concept was then transferred to build a microRNA genosensor. Similar probe length was chosen for the miRNA genosensors, with identical end grafting-modification. The methylene blue redox label, however, did not contain –COH side group as the syntheticDNA probes did. This difference was due to the different labelling approach. The syntheticDNA probes were modified previously in house, while the microRNA probes were purchased already labelled. With the lack of –COH side group, intercalation of label into the duplex base-stack should occur more easily. Furthermore, minimum change was expected by this alteration.

As previously revealed, the miRNA probes was designed with a lower content of C-G bonding in its self-complementary sequence. This lead to a much less stable stem, as reflected from probe's melting temperature. With the less stable stem-loop conformation, higher target affinity should be achieved by the probes, thus improving sensor's detection limit.

microRNA Analysis

microRNA sample analysis is given below. Oligonucleotides were purchased and already modified with methylene blue on its 5' terminus and thiol on its 3' terminus. Two different sequences were used, namely the hsa-mir-618 and hsa-let-7c, exact sequences can be found in table 1, both are also 20-nucleotides long.

Similarly, probes were immobilized as single-stranded DNA on clean gold disk electrode surface through self-assembly. Electrodes used for hsa-mir-618 and hsa-let-7c had electrochemical surface area of 0.062 ± 0.008 cm^2 and 0.088 ± 0.018 cm^2 respectively. Self-assembly was let for 16 hours. Subsequently, electrode was backfilled with 2 mM mercaptohexanol for 30 minutes. Resulting surface coverage for hsa-mir-618 and hsa-let-7c was calculated to be 2.47 ± 0.36 pmol cm^{-2} and 3.52 ± 1.04 pmol cm^{-2} respectively.

Sensor response was calibrated in presence of different concentration of target DNA in range of 0.1 nM to 200 nM. Target strands were diluted serially in 20 mM PBS buffer (pH 7) with 150 mM NaCl and 5 mM MgCl$_2$ to obtain different concentrations. Hybridization was achieved by incubating 10 μL of the target solution on the modified electrodes for 30 minutes. Variability of the sensor was observed from two different electrodes for each sample,

which were equivalently prepared and measured. Calibration measurement used differential pulse voltammetry (DPV) interrogation method with 40 mV modulation amplitude, 10 mV step potential, and scan rate of 20 mV s^{-1}. Measurement was done in deaerated 20 mM PBS buffer (pH 7) with 0.15 M NaCl.

Figure 8.3. Baseline corrected differential pulse voltammograms of the hsa-mir-618 probe, before and after interaction with the complementary target. (inset) Genosensor response across two equivalently prepared electrodes, normalized for the blank, calibrated against DNA concentration.

The sensor started to respond consistently in presence of 70 nM target strands and higher. It was apparent that the sensor was much less sensitive than the synthetic DNA sensor results. Response reached saturation in presence of 100 nM target RNA. Reflecting on the surface coverage and electrode's electrochemical surface area, 173 femtomoles of probes were calculated to be immobilized on the electrode's surface. 10 µL of 100 nM target solution should contain around 1 picomole of target strands. The sensor achieved saturation in presence of (only) 6 fold excess of targets. It was then suggested that hybridization might occur at a more efficient rate, when compared to the syntheticDNA experiment. However, the altered affinity did not seem to have improved sensor's limit of detection.

Similar response pattern was found with the 22-nucleotide hsa-let-7c probes, only to a much smaller magnitude. While limit of detection and saturation point was found to be similar to that of hsa-mir-618, sensors' only generated less than half of the hsa-mir-618 response. This might be caused by sensor's denser surface coverage (calculated at 3.52 ± 1.04 pmol cm^{-2}). The crowded electrode surface could hinder the rotational movement of the duplexes, deterring the MB labels to reach electrode surface.

microRNA in Serum Analysis

Lastly, the sensor's hybridization was tested in presence of complex biological matrix. Target strand for hybridization was diluted in 10% serum and 90% the hybridization usual buffer (20 mM PBS buffer (pH 7) containing 150 mM NaCl and 5 mM MgCl$_2$). The serum used was stored (frozen in -18°C) bovine serum albumin (BSA). Due to time limitation, only one electrode was used for each sample. Other than the hybridization buffer, sensor was fabricated and interrogated in the same way as the previous experiments.

Probes were immobilized as single-stranded DNA on clean gold disk electrode surface through self-assembly. Electrodes used for hsa-mir-618 and hsa-let-7c had electrochemical surface area of 0.0684525 cm^2 and 0.072356 cm^2 respectively. Self-assembly was let for 16 hours. Subsequently, electrode was backfilled with 2 mM mercaptohexanol for 30 minutes. Resulting surface coverage for hsa-mir-618 and hsa-let-7c was calculated to be 2.38 pmol cm^{-2} and 3.03 pmol cm^{-2} respectively.
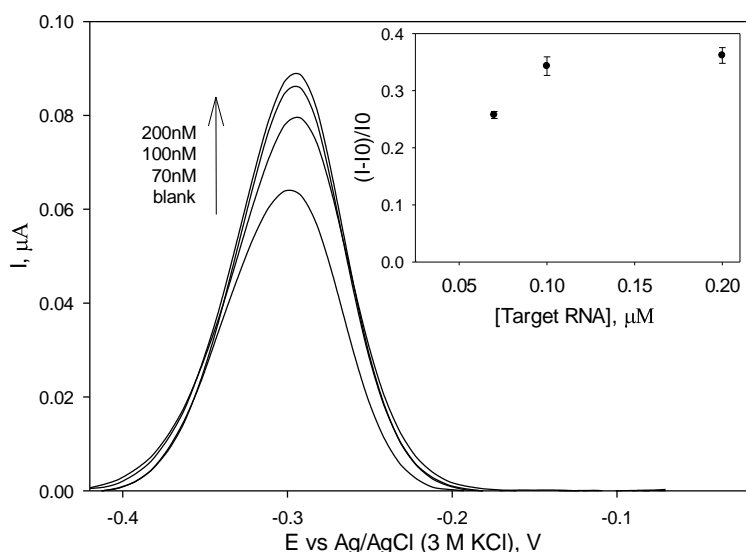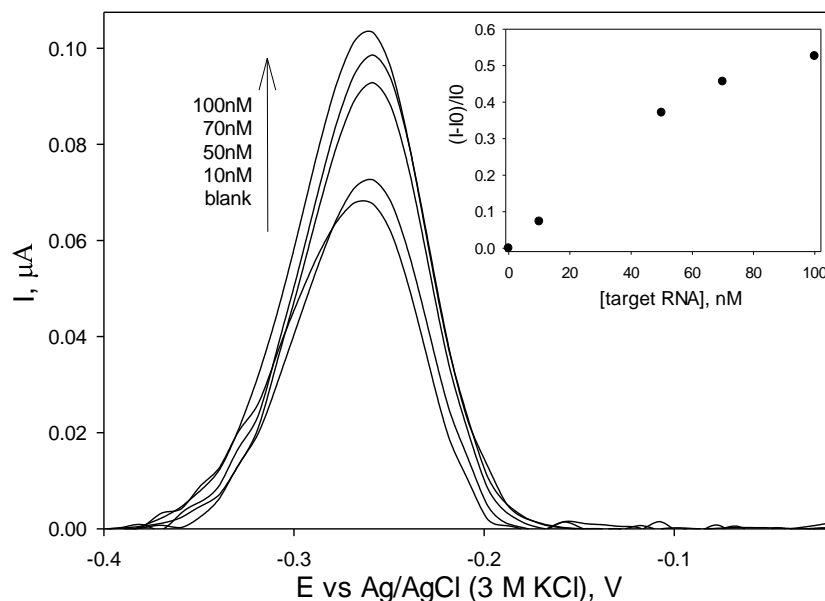

Figure 8.5. Baseline corrected differential pulse voltammograms of the hsa-mir-618 probe in serum, before and after interaction with the complementary target. (inset) Genosensor response across two equivalently prepared electrodes, normalized for the blank, calibrated against DNA concentration.

Interestingly, the hsa-mir-618 sensor performed considerably better in presence of serum. Consistent response was observed starting at a low 10 nM concentration of target. Response showed linear response to the increase of target strands concentration up to 100 nM, the highest concentration used in this experiment.

The effect of serum presence was not examined to its full extent due to limitation in time. The presence of complex biological matrix might have lowered the sensor's effective affinity to target strands. This could in turn

broaden the dynamic range of the sensors. This hypothesis, however, was only based on assumptions. On the other hand, experiment was only performed once. Results reproducibility still need to be visited before it can be concluded.
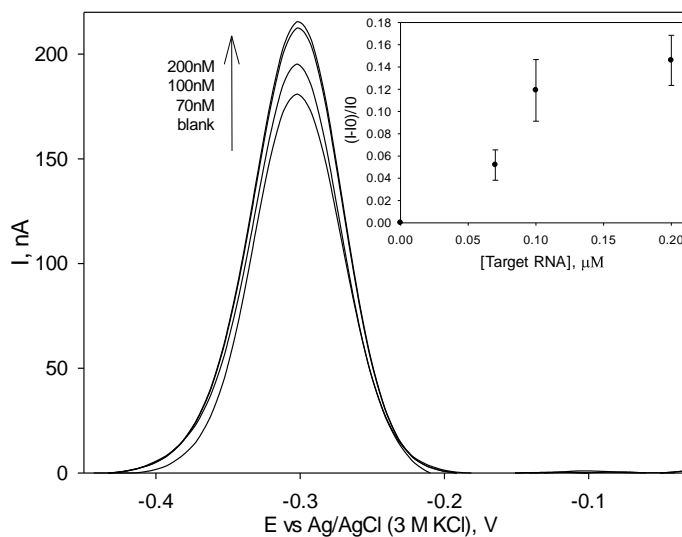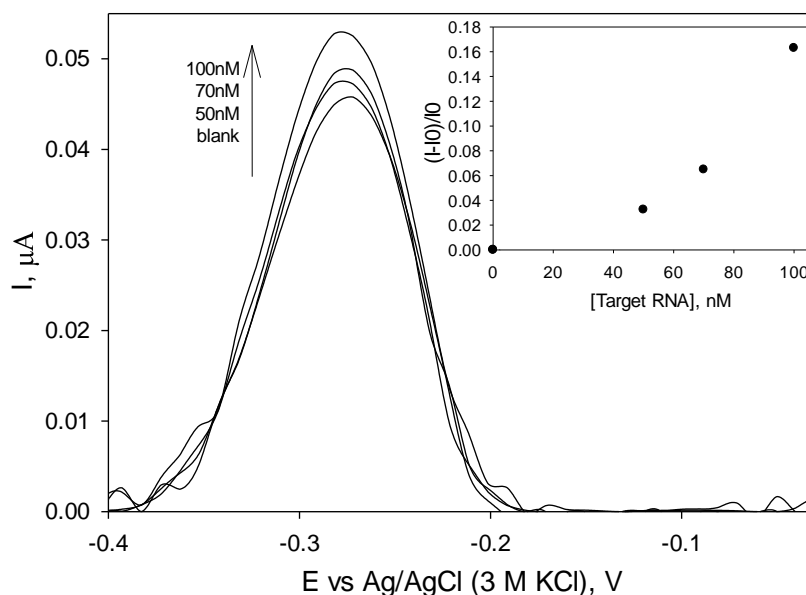

Figure 8.6. Baseline corrected differential pulse voltammograms of the hsa-let-7c probe in serum, before and after interaction with the complementary target. (inset) Genosensor response across two equivalently prepared electrodes, normalized for the blank, calibrated against DNA concentration.

Similarly, the hsa-let-7c sensor's response also seemed to have a broadened dynamic range, where it started to respond consistently when challenged with 50 nM target. The response, however, was still of a much lower magnitude than the response of the hsa-mir-618 sensor. Higher surface coverage of the resulting bioreceptor monolayer was still obtained, despite the adjustment in diluting the incubating solution during self-assembly.

Overall, through the performed serum experiment, it could not be concluded that the sensors performed better in presence of other biological molecules. However, it was rather safe to assume that presence of 10% BSA serum did not disrupt sensing ability of the fabricated genosensor. At 10% serum level, nucleic acid-breaking enzymes (e.g. ribonuclease deoxyribonuclease) did not seem to affect the sensing monolayer of sensor, even in the time frame for 6 incubation sessions, each of 30 minutes.

Chapter 9
Conclusion and Recommendations

Lastly, this chapter concludes the findings of the project and answer the formulated central research question. In answering the central research question, two sub-research questions stated in the first chapter are first to be answered. In the end of the chapter, some recommendations for future works are also put forward.

Experiment results presented in chapter 8 confirmed a genosensor model with reliable, signal-on reporting. The reporting was underlied by hybridization-induced conformational change of the immobilized probes. This conformational change introduced a diffusion-governed agility for the tethered redox label. The redox labels were then facilitated in reaching reach surface electrode. Signal-on reporting has high merit in clinical diagnosis setup for its reliability and unbounded responses. Findings in this project suggested that 20 nucleotide long probes are adequate in achieving such signalling mechanism, irrespective of the sequence. Such signalling was observed to be transferable from a DNA-DNA hybridization system to a DNA-(micro)RNA system. This satisfied generality requirement of clinical genosensing application.

Detection of circulating microRNA biomarker demands a very low limit of detection, down to sub-femtomolar level. Obtained results revealed that such detection limit could not be reached solely by conformational change sensing, when interrogated with electrochemistry's differential pulse voltammetry method. Increasing affinity between probes and target strands (by around two-fold) was not observed to result in an improved limit of detection.

Hence, the central research question can be answered.

'*How can genosensor be applied to detect microRNA hypoxia biomarkers for clinical diagnosis purpose?*'

Reliable genosensor signalling can be achieved through the depicted conformational change sensing. However, genosensor's sensitivity was still proven to be insufficient for clinical diagnosis applications.

In general, the proposed sensing system possesses apparent advantages over the traditional immunohistochemistry assay; e.g. in terms of speed of diagnosis, versatility, and labour-/instrumentation requirement. Therefore it is of great value to continue such work, mostly in improvement of sensor's detection limit.

Amendment of probes' thermodynamics and affinity to targets are area worth further exploring. The use of engineered nucleic acid polymers should boost limit of detection for their significantly higher hybridization affinity.

The direct affinity between probes and targets also suggests that limit of detection can be improved by increasing the sample size. The used 10 µL sample volume was minute even for real biological samples. Therefore it should not be a problem to increase this sample size. To aid this, a bigger electrode might be necessary. Furthermore, signal amplification can also be useful means in improving sensor's sensitivity and limit of detection. Amplification can be achieved through electrocatalysis, by using electron transfer intermediaries to carry out redox reaction of the label away from the electrode surface. On the other hand, this might underplay the commercially and POC attractive reagentless trait.

References

[1]   J. M. Brown and A. J. Giaccia, "The Unique Physiology of Solid Tumors : Opportunities (and Problems) for Cancer Therapy," *Cancer Res.*, vol. 58, no. 9, pp. 1408–1416, 1998.

[2]   C. Devlin, S. Greco, F. Martelli, and M. Ivan, "MiR-210: More than a silent player in hypoxia," *IUBMB Life*, vol. 63, no. 2, pp. 94–100, 2011.

[3]   W. R. Wilson and M. P. Hay, "Targeting hypoxia in cancer therapy," *Nat. Rev. Cancer*, vol. 11, no. 6, pp. 393–410, 2011.

[4]   R. K. Jain, "Normalization of tumor vasculature: an emerging concept in antiangiogenic therapy.," *Science*, vol. 307, no. 5706, pp. 58–62, 2005.

[5]   S. Greco and F. Martelli, "MicroRNAs in Hypoxia Response," *Antioxid. Redox Signal.*, vol. 21, no. 8, pp. 1164–1166, 2014.

[6]   J. Zhou, T. Schmid, S. Schnitzer, and B. Brüne, "Tumor hypoxia and cancer progression," *Cancer Lett.*, vol. 237, no. 1, pp. 10–21, 2006.

[7]   M. Höckel and P. Vaupel, "Tumor hypoxia: definitions and current clinical, biologic, and molecular aspects.," *J. Natl. Cancer Inst.*, vol. 93, no. 4, pp. 266–276, 2001.

[8]   "Tissue Hypoxia - How to Detect, How to Correct, How to Prevent," *Am. J. Respir. Crit. Care Med.*, vol. 154, pp. 1573–1578, 1996.

[9]   A. P. N. Skubitz, "Immunohistochemical staining : A technique used to localize Immunohistochemisty (IHC) Immunohistochemisty (IHC) KWRIS Mini-Med School," 2013.

[10]   R. Kulshreshtha, R. V Davuluri, G. a Calin, and M. Ivan, "A microRNA component of the hypoxic response.," *Cell Death Differ.*, vol. 15, no. 4, pp. 667–671, 2008.

[11]   N. C. Institute, "NCI Dictionary of Cancer Terms," *http://www.cancer.gov/publications/dictionaries/cancer-terms/?CdrID=45618*. .

[12]   A. Mishra and M. Verma, "Cancer biomarkers: Are we ready for the prime time?," *Cancers (Basel).*, vol. 2, no. 1, pp. 190–208, 2010.

[13]   H. Lodish, a. Berk, and S. L. Z. E. Al., *Molecular Cell Biology*. 2000.

[14]   F. Crick, "Central Dogma of Molecular Biology," *Nature*, vol. 227, no. 8, pp. 561–563, 1970.

[15]   J. D. Watson and F. H. C. Crick, "Molecular structure of nucleic acids," *Nature*, vol. 171, no. 4356. pp. 737–738, 1953.

[16]   Lodish H, B. A, Z. SL, and E. Al, "Structure of Nucleic Acids," in *Molecular Cell Biology*, 4th ed., New York: W. H. Freeman, 2000.

[17]   E. T. Kool, "Hydrogen Bonding, Base Stacking, and Steric Effects in DNA Replication," *Annu. Rev. Biophys. Biomol. Struct.*, vol. 30, no. October, pp. 1–22, 2001.

[18]   C. J. Murphy, M. R. Arkin, Y. Jenkins, N. D. Ghatlia, S. H. Bossmann, N. J. Turro, and J. K. Barton, "Long-range photoinduced electron transfer through a DNA helix.," *Science*, vol. 262, no. 5136, pp. 1025–1029, 1993.

[19]   Y. He, T. Ye, M. Su, C. Zhang, A. E. Ribbe, W. Jiang, and C. Mao, "Hierarchical self-assembly of DNA into symmetric supramolecular polyhedra.," *Nature*, vol. 452, no. 7184, pp. 198–201, 2008.

[20]   E. Braun, Y. Eichen, U. Sivan, and G. Ben-Yoseph, "DNA-templated assembly and electrode attachment of a conducting silver wire.," *Nature*, vol. 391, no. 6669, pp. 775–778, 1998.

[21]   E. M. Boon, D. M. Ceres, T. G. Drummond, M. G. Hill, and J. K. Barton, "Mutation detection by electrocatalysis at DNA-modified electrodes.," *Nat. Biotechnol.*, vol. 18, no. 10, pp. 1096–1100, 2000.

[22]   A. A. Gorodetsky, M. C. Buzzeo, and J. K. Barton, "DNA-Mediated Electrochemistry," *Bioconjug. Chem.*, vol. 19, no. 12, 2008.

[23]   M. W. Wright and E. a Bruford, "Naming 'junk': human non-protein coding RNA (ncRNA) gene nomenclature.," *Hum. Genomics*, vol. 5, no. 2, pp. 90–98, 2011.

[24]   V. Ambros, "The functions of animal microRNAs.," *Nature*, vol. 431, no. 7006, pp. 350–355, 2004.

[25]   E. Alerting, "MicroRNA function : Multiple mechanisms for a tiny RNA ? MicroRNA function : Multiple mechanisms for a tiny RNA ?," no. Bartel 2004, pp. 1753–1761, 2005.

[26]   L.-A. Macfarlane and P. R. Murphy, "MicroRNA: Biogenesis, Function and Role in Cancer.," *Curr. Genomics*, vol. 11, no. 7, pp. 537–561, 2010.

[27]   R. C. Lee, "The C . elegans Heterochronic Gene lin-4 Encodes Small RNAs with Antisense Complementarity to & II-14," *Cell*, vol. 75, pp. 843–854, 1993.

[28]   S. L. Ameres and P. D. Zamore, "Diversifying microRNA sequence and function.," *Nat. Rev. Mol. Cell Biol.*, vol. 14, no. 8, pp. 475–88, 2013.

[29]   A. M. Ardekani and M. M. Naeini, "The role of microRNAs in human diseases," *Avicenna J. Med. Biotechnol.*, vol. 2, no. 4, pp. 161–179, 2010.

[30]   P. S. Mitchell, R. K. Parkin, E. M. Kroh, B. R. Fritz, S. K. Wyman, E. L. Pogosova-Agadjanyan, A. Peterson, J. Noteboom, K. C. O'Briant, A. Allen, D. W. Lin, N. Urban, C. W. Drescher, B. S. Knudsen, D. L. Stirewalt, R. Gentleman, R. L. Vessella, P. S. Nelson, D. B. Martin, and M. Tewari, "Circulating microRNAs as stable blood-based markers for cancer detection.," *Proc. Natl. Acad. Sci. U. S. A.*, vol. 105, no. 30, pp. 10513–10518, 2008.

[31]   K. C. Vickers, B. T. Palmisano, B. M. Shoucri, R. D. Shamburek, and A. T. Remaley, "MicroRNAs are transported in plasma and delivered to recipient cells by high-density lipoproteins.," *Nat. Cell Biol.*, vol. 13, no. 4, pp. 423–433, 2011.

[32]   A. Zernecke, K. Bidzhekov, H. Noels, E. Shagdarsuren, L. Gan, B. Denecke, M. Hristov, T. Köppel, M. N. Jahantigh, E. Lutgens, S. Wang, E. N. Olson, A. Schober, and C. Weber, "Delivery of microRNA-126 by apoptotic bodies induces CXCL12-dependent vascular protection.," *Sci. Signal.*, vol. 2, no. 100, p. ra81, 2009.

[33]   M. Tsujiura, D. Ichikawa, S. Komatsu, a Shiozaki, H. Takeshita, T. Kosuga, H. Konishi, R. Morimura, K. Deguchi, H. Fujiwara, K. Okamoto, and E. Otsuji, "Circulating microRNAs in plasma of patients with gastric cancers.," *Br. J. Cancer*, vol. 102, no. 7, pp. 1174–1179, 2010.

[34]   M. C. Brahimi-Horn, J. Chiche, and J. Pouysségur, "Hypoxia and cancer," *J. Mol. Med.*, vol. 85, no. 12, pp. 1301–1307, 2007.

[35]   C. Wu, J. So, B. N. Davis-Dusenbery, H. H. Qi, D. B. Bloch, Y. Shi, G. Lagna, and a. Hata, "Hypoxia Potentiates MicroRNA-Mediated Gene Silencing through Posttranslational Modification of Argonaute2," *Mol. Cell. Biol.*, vol. 31, no. 23, pp. 4760–4774, 2011.

[36]   R. Kulshreshtha, M. Ferracin, S. E. Wojcik, R. Garzon, H. Alder, F. J. Agosto-Perez, R. Davuluri, C.-G. Liu, C. M. Croce, M. Negrini, G. a Calin, and M. Ivan, "A microRNA signature of hypoxia.," *Mol. Cell. Biol.*, vol. 27, no. 5, pp. 1859–1867, 2007.

[37]   G. Shen, X. Li, Y. Jia, G. a Piazza, and Y. Xi, "Hypoxia-regulated microRNAs in human cancer.," *Acta Pharmacol. Sin.*, vol. 34, no. 3, pp. 336–41, 2013.

[38]   Y. Xiao, R. Y. Lai, and K. W. Plaxco, "Preparation of electrode-immobilized, redox-modified oligonucleotides for electrochemical DNA and aptamer-based sensing.," *Nat. Protoc.*, vol. 2, no. 11, pp. 2875–2880, 2007.

[39]   M. Aizawa, a. Morioka, S. Suzuki, and Y. Nagamura, "Enzyme immunosenser III. Amperometric determination of human cherienic gonadotropin by membrane-bound antibody," *Anal. Biochem.*, vol. 94, no. 1, pp. 22–28, 1979.

[40]   L. C. Clark and C. Lyons, "Electrode systems for continuous monitoring in cardiovascular surgery," *Ann. N. Y. Acad. Sci.*, vol. 102, no. 1, pp. 29–45, 1962.

[41]   Y. Xiao, F. Patolsky, E. Katz, J. F. Hainfeld, and I. Willner, "'Plugging into Enzymes': nanowiring of redox enzymes by a gold nanoparticle.," *Science*, vol. 299, no. 5614, pp. 1877–1881, 2003.

[42]   S. Tyagi and F. R. Kramer, "Molecular Beacons: Probes that Fluoresce upon Hybridization," *Nat. Biotechnol.*, vol. 14, no. 3, pp. 303–308, 1996.

[43]   W. H. King, "Piezoelectric Sorption Detector.," *Anal. Chem.*, vol. 36, no. 9, pp. 1735–1739, 1964.

[44]   C. Fan, K. W. Plaxco, and A. J. Heeger, "Electrochemical interrogation of conformational changes as a reagentless method for the sequence-specific detection of DNA.," *Proc. Natl. Acad. Sci. U. S. A.*, vol. 100, no. 16, pp. 9134–9137, 2003.

[45]   T. G. Drummond, T. G. Drummond, M. G. Hill, M. G. Hill, J. K. Barton, and J. K. Barton, "Electrochemical DNA sensors.," *Nat. Biotechnol.*, vol. 21, no. 10, pp. 1192–9, 2003.

[46]   E. Hamidi-Asl, E. Hasheminejad, and M. Mascini, "A review on the electrochemical biosensors for determination of microRNAs," *Talanta*, vol. 115, pp. 74–83, 2013.

[47]   K. B. Mullis, "The unusual origin of the polymerase chain reaction.," *Sci. Am.*, vol. 262, no. 4, pp. 56–61, 64–65, 1990.

[48]   U. Champaign, "Polymerase Chain Reaction," *Brenner's Encycl. Genet. Second Ed.*, vol. 5, no. 3, pp. 392–395, 2013.

[49]   J. P. Tosar, G. Brañas, and J. Laíz, "Electrochemical DNA hybridization sensors applied to real and complex biological samples," *Biosens. Bioelectron.*, vol. 26, no. 4, pp. 1205–1217, 2010.

[50]   W. M. Freeman, S. J. Walker, and K. E. Vrana, "Quantitative RT-PCR: Pitfalls and potential," *Biotechniques*, vol. 26, no. 1, pp. 112–125, 1999.

[51]   F. S. Collins, A. Patrinos, E. Jordan, A. Chakravarti, R. Gesteland, and L. Walters, "New goals for the U.S. Human Genome Project: 1998-2003," *Science*, vol. 282, no. 5389, pp. 682–689, 1998.

[52]   M. P. Sawicki, G. Samara, M. Hurwitz, and E. Passaro, "Human Genome Project," *Am. J. Surg.*, vol. 165, no. 2, pp. 258–264, 1993.

[53]   J. a. Johnson, "Pharmacogenetics: Potential for individualized drug therapy through genetics," *Trends Genet.*, vol. 19, no. 11, pp. 660–666, 2003.

[54]   V. Gubala, L. F. Harris, A. J. Ricco, M. X. Tan, and D. E. Williams, "Point of care diagnostics: Status and future," *Anal. Chem.*, vol. 84, no. 2, pp. 487–515, 2012.

[55]   J. F. Rusling, C. V Kumar, J. S. Gutkind, and V. Patel, "Measurement of biomarker proteins for point-of-care early detection and monitoring of cancer.," *Analyst*, vol. 135, no. 10, pp. 2496–2511, 2010.

[56]   A. W. Wark, H. J. Lee, and R. M. Corn, "Multiplexed Detection Methods for Profiling microRNA Expression in Biological Samples," *Angew Chem Int Ed.*, vol. 47, no. 4, pp. 644–652, 2008.

[57]   A. P. Abel, M. G. Weller, G. L. Duveneck, M. Ehrat, and H. M. Widmer, "Fiber-optic evanescent wave biosensor for the detection of oligonucleotides," *Anal. Chem.*, vol. 68, no. 17, pp. 2905–2912, 1996.

[58]   X. Fang, X. Liu, S. Schuster, and W. Tan, "Designing a novel molecular beacon for surface-immobilized DNA hybridization studies," *J. Am. Chem. Soc.*, vol. 121, no. 12, pp. 2921–2922, 1999.

[59]   J. Homola, "Present and future of surface plasmon resonance biosensors," *Anal. Bioanal. Chem.*, vol. 377, no. 3, pp. 528–539, 2003.

[60]   D.-K. Xu, L.-R. Ma, Y.-Q. Liu, Z.-H. Jiang, and Z.-H. Liu, "Development of chemiluminescent biosensing of nucleic acids based on oligonucleotide-immobilized gold surfaces," *Analyst*, vol. 124, no. 4, pp. 533–536, 1999.

[61]   V. Pavlov, Y. Xiao, R. Gill, A. Dishon, M. Kotler, and I. Willner, "Amplified Chemiluminescence Surface Detection of DNA and Telomerase Activity Using Catalytic Nucleic Acid Labels," *Anal. Chem.*, vol. 76, no. 7, pp. 2152–2156, 2004.

[62]   M. Yang, C. Liu, K. Qian, P. He, and Y. Fang, "Study on the electrochemiluminescence behavior of ABEI and its application in DNA hybridization analysis.," *Analyst*, vol. 127, no. 9, pp. 1267–1271, 2002.

[63]   B. G. Healey, R. S. Matson, and D. R. Walt, "Fiberoptic DNA sensor array capable of detecting point mutations.," *Anal. Biochem.*, vol. 251, no. 2, pp. 270–279, 1997.

[64]   M. You, C. Yang, and W. Tan, "Molecular Beacons for Detection of Single-Nucleotide Polymorphisms," in *Molecular Beacons SE - 4*, C. J. Yang and W. Tan, Eds. Springer Berlin Heidelberg, 2013, pp. 61–74.

[65]   M. M. Mhlanga and L. Malmberg, "Using molecular beacons to detect single-nucleotide polymorphisms with real-time PCR.," *Methods*, vol. 25, no. 4, pp. 463–471, 2001.

[66]   A. W. Peterson, R. J. Heaton, and R. M. Georgiadis, "The effect of surface probe density on DNA hybridization.," *Nucleic Acids Res.*, vol. 29, no. 24, pp. 5163–5168, 2001.

[67]   Wikipedia, "Surface plasmon resonance," *Wikimedia*. .

[68]   C. K. O'sullivan and G. G. Guilbault, "Commercial quartz crystal microbalances–theory and applications," *Biosens. Bioelectron.*, vol. 14, no. 8, pp. 663–670, 1999.

[69]   N. C. Fawcett, J. a. Evans, L.-C. Chien, and N. Flowers, "Nucleic Acid Hybridization Detected by Piezoelectric Resonance," *Anal. Lett.*, vol. 21, no. 7, pp. 1099–1114, 1988.

[70]   F. Patolsky, A. Lichtenstein, and I. Willner, "Amplified microgravimetric quartz-crystal-microbalance assay of DNA using oligonucleotide-functionalized liposomes or biotinylated liposomes," *J. Am. Chem. Soc.*, vol. 122, no. 2, pp. 418–419, 2000.

[71]   I. Willner, F. Patolsky, Y. Weizmann, and B. Willner, "Amplified detection of single-base mismatches in DNA using microgravimetric quartz-crystal-microbalance transduction," *Talanta*, vol. 56, no. 5, pp. 847–856, 2002.

[72]   A. J. Bard and L. R. Faulkner, *Electrochemical methods : fundamentals and applications*. 2001.

[73]   S. Minteer and G. Brisard, "Physical and Analytical Electrochemistry : The Fundamental Core of Electrochemistry," *Electrochem. Soc. Interface*, pp. 62–65, 2006.

[74]   J. Wang, "Electrochemical nucleic acid biosensors," *Anal. Chim. Acta*, vol. 469, no. 1, pp. 63–71, 2002.

[75]   S. Cagnin, M. Caraballo, C. Guiducci, P. Martini, M. Ross, M. SantaAna, D. Danley, T. West, and G. Lanfranchi, "Overview of Electrochemical DNA Biosensors: New Approaches to Detect the Expression of Life," *Sensors*, vol. 9, no. 4, pp. 3122–3148, 2009.

[76]   E. Palecek, "Oscillographic Polarography of Highly Polymerized Deoxyribonucleic Acid," *Nature*, vol. 188, pp. 656–657, 1960.

[77]   C. E. Crespo-Hernández, D. M. Close, L. Gorb, and J. Leszczynski, "Determination of redox potentials for the Watson-crick base pairs, DNA nucleosides, and relevant nucleoside analogues," *J. Phys. Chem. B*, vol. 111, no. 19, pp. 5386–5395, 2007.

[78]   D. H. Johnston, K. C. Glasgow, and H. H. Thorp, "Electrochemical Measurement of the Solvent Accessibility of Nucleobases Using Electron Transfer between DNA and Metal Complexes," *J. Am. Chem. Soc.*, vol. 117, no. 35, pp. 8933–8938, 1995.

[79] H. H. Thorp, "Reagentless detection of DNA sequences on chemically modified electrodes," *Trends Biotechnol.*, vol. 21, no. 12, pp. 522–524, 2003.

[80] E. G. Hvastkovs and D. a Buttry, "Recent advances in electrochemical DNA hybridization sensors.," *Analyst*, vol. 135, no. 8, pp. 1817–1829, 2010.

[81] M. Fojta, M. Fojta, L. Havran, L. Havran, S. Billova, S. Billova, P. Kostecka, P. Kostecka, M. Masarik, M. Masarik, R. Kizek, and R. Kizek, "Two-Surface Strategy in Electrochemical DNA Hybridization Assays: Detection of Osmium-Labeled Target DNA at Carbon Electrodes," *Electroanalysis*, vol. 15, no. 5–6, pp. 431–440, 2003.

[82] M. Dequaire and A. Heller, "Screen printing of nucleic acid detecting carbon electrodes," *Anal. Chem.*, vol. 74, no. 17, pp. 4370–4377, 2002.

[83] M. Ozsoz, A. Erdem, K. Kerman, D. Ozkan, B. Tugrul, N. Topcuoglu, H. Ekren, and M. Taylan, "Electrochemical genosensor based on colloidal gold nanoparticles for the detection of Factor V Leiden mutation using disposable pencil graphite electrodes," *Anal. Chem.*, vol. 75, no. 9, pp. 2181–2187, 2003.

[84] Z. Gao, "A highly sensitive electrochemical assay for microRNA expression profiling," *Analyst*, vol. 137, no. 7, p. 1674, 2012.

[85] C. G. Pheeney and J. K. Barton, "DNA electrochemistry with tethered methylene blue," *Langmuir*, vol. 28, no. 17, pp. 7063–7070, 2012.

[86] X. Luo and I. M. Hsing, "Immobilization-free multiplex electrochemical DNA and SNP detection," *Biosens. Bioelectron.*, vol. 25, no. 4, pp. 803–808, 2009.

[87] P. Nielsen, M. Egholm, R. . Berg, and O. Buchardt, "Sequence-selective recognition of DNA by strand displacement with a thymine-substituted polyamide," *Science (80-.).*, vol. 254, pp. 1497–1500, 1991.

[88] R. C. Alkire, D. M. Kolb, J. Lipkowski, and P. N. Ross, *Bioelectrochemistry: Fundamentals, Applications and Recent Developments*. Weinheim: Wiley-VCH, 2011.

[89] T. Goda, A. B. Singi, Y. Maeda, A. Matsumoto, M. Torimura, H. Aoki, and Y. Miyahara, "Label-free potentiometry for detecting DNA hybridization using peptide nucleic acid and DNA probes.," *Sensors (Basel).*, vol. 13, no. 2, pp. 2267–78, 2013.

[90] M. T. Carter, "Pulse Voltammetry," *J. Chem. Educ.*, vol. 60, no. 4, pp. 296–298, 1983.

[91] T. Kissinger and W. Heineman, "Cyclic Voltammetry," *J. Chem. Educ.*, no. 2, pp. 702–706, 2010.

[92] F. Yusoff, N. Mohamed, A. Aziz, and S. A. Ghani, "Electrocatalytic Reduction of Oxygen at Perovskite (BSCF)-MWCNT Composite Electrodes," *Mater. Sci. Appl.*, vol. 05, no. 04, pp. 199–211, 2014.

[93] J. Wengel, A. Koshkinalb, S. K. Singh, P. Nielsenc, M. Meldgaard, V. K. Rajwanshi, R. Kumara, J. Skouvd, C. B. Nielsenc, J. P. Jacobsen, N. Jacobsenb, C. E. Olsene, and D.- Copenhagen, "LNA (LOCKED NUCLEIC ACID) Jesper Wengel'**, Alexei Koshkinalb, Sanjay K. Singh', Poul Nielsenc, Michael Meldgaard', Vivek K. Rajwanshi', Ravindra Kumara, Jan Skouvd Christina B. Nielsenc, Jens Peter Jacobsen', Nana Jacobsenb, and Carl E. Olsene," vol. 18, no. 1 999, pp. 1365–1370, 1999.

[94]   J. K. Watts, "Locked nucleic acid: tighter is different," *Chem Commun*, vol. 49, no. 50, pp. 5618–5620, 2013.

[95]   T. Takiya, Y. Seto, H. Yasuda, T. Suzuki, and K. Kawai, "An empirical approach for thermal stability (Tm) prediction of PNA/DNA duplexes.," *Nucleic Acids Symp. Ser. (Oxf).*, no. 48, pp. 131–132, 2004.

[96]   A. Abi and E. E. Ferapontova, "Electroanalysis of single-nucleotide polymorphism by hairpin DNA architectures," *Anal. Bioanal. Chem.*, vol. 405, no. 11, pp. 3693–3703, 2013.

[97]   W. Yang and R. Y. Lai, "Comparison of the stem-loop and linear probe-based electrochemical DNA sensors by alternating current voltammetry and cyclic voltammetry," *Langmuir*, vol. 27, no. 23, pp. 14669–14677, 2011.

[98]   F. Ricci, R. Y. Lai, and K. W. Plaxco, "Linear, redox modified DNA probes as electrochemical DNA sensors.," *Chem. Commun. (Camb).*, no. 36, pp. 3768–3770, 2007.

[99]   D. Kang, A. Vallée-Bélisle, A. Porchetta, K. W. Plaxco, and F. Ricci, "Re-engineering electrochemical biosensors to narrow or extend their useful dynamic range," *Angew. Chemie - Int. Ed.*, vol. 51, no. 27, pp. 6717–6721, 2012.

[100]   A. Hulanicki and S. Glab, "Redox indicators. Characteristics and applications," *Pure Appl. Chem.*, vol. 50, no. 5, pp. 463–498, 1978.

[101]   E. Farjami, R. Campos, and E. E. Ferapontova, "Effect of the DNA end of tethering to electrodes on electron transfer in methylene blue-labeled DNA duplexes," *Langmuir*, vol. 28, no. 46, pp. 16218–16226, 2012.

[102]   F. Lucarelli, G. Marrazza, a. P. F. Turner, and M. Mascini, "Carbon and gold electrodes as electrochemical transducers for DNA hybridisation sensors," *Biosens. Bioelectron.*, vol. 19, no. 6, pp. 515–530, 2004.

[103]   E. Palecek and M. Fojta, "Detecting DNA Hybridization and Damage," *Anal. Chem.*, vol. 73, no. 3, p. 74A–84A, 2001.

[104]   R. G. Nuzzo and D. L. Allara, "Adsorption of bifunctional organic disulfides on gold surfaces," *J. Am. Chem. Soc.*, vol. 105, no. 11, pp. 4481–4483, 1983.

[105]   M. M. S. Silva, I. T. Cavalcanti, M. F. Barroso, M. G. F. Sales, and R. F. Dutra, "Gold electrode modified by self-assembled monolayers of thiols to determine DNA sequences hybridization," *J. Chem. Sci.*, vol. 122, no. 6, pp. 911–917, 2010.

[106]   D. V Leff, L. Brandt, and J. R. Heath, "Synthesis and Characterization of Hydrophobic, Organically- Soluble Gold Nanocrystals Functionalized with Primary Amines," *Langmuir*, vol. 12, no. c, pp. 4723–4730, 1996.

[107]   T. M. Herne and M. J. Tarlov, "Characterization of DNA probes immobilized on gold surfaces," *J Am Chem Soc*, vol. 119, no. 38, pp. 8916–8920, 1997.

[108]   A. V. Ladik, F. M. Geiger, and S. R. Walter, "Immobilization of DNA onto Gold and Dehybridization of Surface-Bound DNA on Glass," *Nanoscape*, vol. 7, no. 1, pp. 19–23, 2010.

[109]   C. Boozer, S. Chen, and S. Jiang, "Controlling DNA orientation on mixed ssDNA/OEG SAMs," *Langmuir*, vol. 22, no. 10, pp. 4694–4698, 2006.

[110] J. N. Murphy, A. K. H. Cheng, H. Z. Yu, and D. Bizzotto, "On the nature of DNA self-assembled monolayers on Au: Measuring surface heterogeneity with electrochemical in situ fluorescence microscopy," *J. Am. Chem. Soc.*, vol. 131, no. 11, pp. 4042–4050, 2009.

[111] T. Doneux, A. De Rache, E. Triffaux, A. Meunier, M. Steichen, and C. Buess-Herman, "Optimization of the Probe Coverage in DNA Biosensors by a One-Step Coadsorption Procedure," *ChemElectroChem*, vol. 1, no. 1, pp. 147–157, 2014.

[112] A. Ulman, "Formation and Structure of Self-Assembled Monolayers," *Chem. Rev.*, vol. 96, no. 4, pp. 1533–1554, 1996.

[113] E. Farjami, L. Clima, K. Gothelf, and E. E. Ferapontova, "'Off-On' electrochemical hairpin-DNA-based genosensor for cancer diagnostics," *Anal. Chem.*, vol. 83, no. 5, pp. 1594–1602, 2011.

[114] K. B. Cederquist, R. S. Golightly, and C. D. Keating, "Molecular beacon-metal nanowire interface: Effect of probe sequence and surface coverage on sensor performance," *Langmuir*, vol. 24, no. 16, pp. 9162–9171, 2008.

[115] W. Yang, J. Y. Gerasimov, and R. Y. Lai, "Folding-based electrochemical DNA sensor fabricated on a gold-plated screen-printed carbon electrode.," *Chem. Commun. (Camb).*, no. 20, pp. 2902–2904, 2009.

[116] C. E. Immoos, S. J. Lee, and M. W. Grinstaff, "DNA-PEG-DNA triblock macromolecules for reagentless DNA detection," *J. Am. Chem. Soc.*, vol. 126, no. 35, pp. 10814–10815, 2004.

[117] Y. Wu and R. Y. Lai, "Effects of DNA Probe and Target Flexibility on the Performance of a 'Signal-on' Electrochemical DNA Sensor.," *Anal. Chem.*, 2014.

[118] Research Solutions & Resources LLC, "Potentials of Common Reference Electrodes," *http://www.consultrsr.net/resources/ref/refpotls.htm#ref*. .

[119] E. P. Friis, J. E. T. Andersen, L. L. Madsen, N. Bonander, P. Møller, and J. Ulstrup, "Dynamics of Pseudomonas aeruginosa azurin and its Cys3Ser mutant at single-crystal gold surfaces investigated by cyclic voltammetry and atomic force microscopy," *Electrochim. Acta*, vol. 43, no. 9, pp. 1114–1122, 1998.

[120] N. R. Markham and M. Zuker, "DINAMelt web server for nucleic acid melting prediction," *Nucleic Acids Res.*, vol. 33, no. SUPPL. 2, pp. 577–581, 2005.

[121] N. R. Markham and M. Zuker, "UNAFold Software for nucleic acid folding and hybridization," vol. 453, no. 1, 2008.

[122] P. a E. Piunno, J. Watterson, C. C. Wust, and U. J. Krull, "Considerations for the quantitative transduction of hybridization of immobilized DNA," *Anal. Chim. Acta*, vol. 400, no. 1–3, pp. 73–89, 1999.

[123] K. a. Peterlinz, R. M. Georgiadis, T. M. Herne, and M. J. Tarlov, "Observation of hybridization and dehybridization of thiol-tethered DNA using two-color surface plasmon resonance spectroscopy," *J. Am. Chem. Soc.*, vol. 119, no. 14, pp. 3401–3402, 1997.

[124] L. M. Fischer, M. Tenje, A. R. Heiskanen, N. Masuda, J. Castillo, A. Bentien, J. Émneus, M. H. Jakobsen, and A. Boisen, "Gold cleaning methods for electrochemical detection applications," *Microelectron. Eng.*, vol. 86, no. 4–6, pp. 1282–1285, 2009.
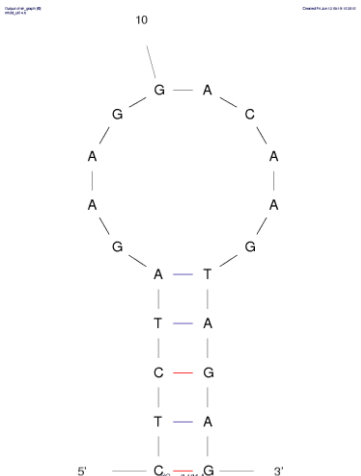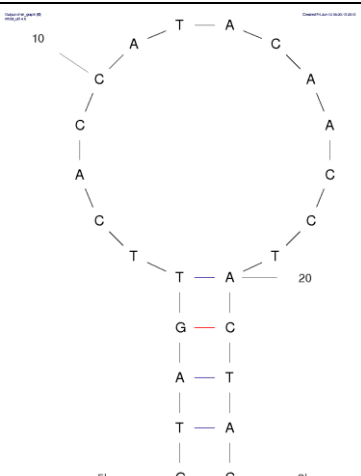
[125]   J. P. Hoare, "A Cyclic Voltammetric Study of the Gold-Oxygen System," *J. Electrochem. Soc.*, vol. 131, no. 8, p. 1808, 1984.

[126]   S. Chemicals, "Tris(3-hydroxypropyl)phosphine and Tris(2-carboxyethyl)phosphinehydrochloride: disulfide reducing agents for molecular diagnostics."

[127]   A. H. Suroviec, "Determining Surface Coverage of Self-Assembled Monolayers on Gold Electrodes," *Chem Educ.*, vol. 4171, no. 12, pp. 83–85, 2012.

[128]   D. Harvey, "Voltammetric Methods." .

[129]   N. R. Markham, "DI-Nucleic Acid hybridization and melting prediction," *http://mfold.rna.albany.edu/?q=DINAMelt*. .

[130]   P. N. Borer, B. Dengler, I. Tinoco, and O. C. Uhlenbeck, "Stability of ribonucleic acid double-stranded helices.," *J. Mol. Biol.*, vol. 86, no. 4, pp. 843–853, 1974.

Appendices

Appendix A
DNA/RNA Foldings

This part visualizes the foldings of the sequences used in the project. Folding simulation was done by DINAmelt quickmelt algorithm [129]. The schematics presented the differences in the self-complementary/stems between the probes in the more apparent way. From the table below, the direct relation between stem's composition and probe's melting temperature are evident.

Type	Oligo Name	Foldings in 20 mM PBS (pH 7)/0.150 M NaCl/0.005 M MgCl$_2$	Melting Temperature
DNA probe	DNA hairpin hsa-mir-618		38.0°C
DNA probe	DNA hairpin hsa-let-7c		37.0°C

<table>
<tr><td>DNA probe</td><td>SyntheticDNA hairpin</td><td></td><td>55.3°C</td></tr>
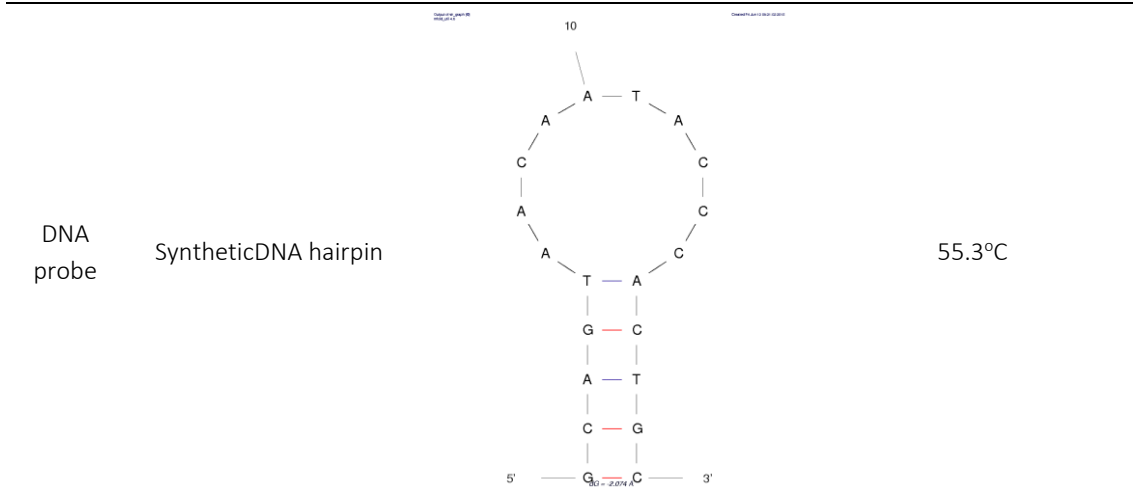</table>

Table A.1. Foldings of DNA probes in 20 mM PBS (pH 7) containing 150 mM NaCl and 5 mM MgCl$_2$, generated by DINAmelt [129]

Targets also form hairpin structure which can compete with hybridization with probes. Therefore the folding and melting temperature were also analysed to ensure that the probe-target hybrids are the more thermodynamically favourable state.

Type	Oligo Name	Foldings	Melting Temperature
		in 20 mM PBS (pH 7)/0.150 M NaCl/0.005 M MgCl$_2$	
DNA target	cDNA hsa-mir-618		36°C
DNA target	cDNA hsa-let-7c		39.7°C

RNA target	cRNA hsa-mir-618		54°C
RNA target	cRNA hsa-let-7c		55.9°C
DNA target	SyntheticDNA hairpin		56.4°C

Table A.2. Foldings of target strands in 20 mM PBS (pH 7)/150 mM NaCl/5 mM MgCl₂, generated by DINAmelt quickfold algorithm [129]

57

Appendix B
Experimental Results

This chapter presents various experimental results, as previously referred to in the main content of the report. Each experiments are elaborated and introduced separately.

1.   Mercaptohexanol-modified gold electrode

This chapter presents the results of control experiments aimed to ensure that the backfilling agent used in the sensor did not introduce interfering effects. Figure B.1 shows the cyclic voltammogram of the gold electrode modified only with mercaptohexanol monolayer. Electrode was modified through self-assembly of 2 mM thiolated mercaptohexanol in 20 mM PBS (pH 7) buffer with 150 mM NaCl for 30 minutes. Measurement was also done in 20 mM PBS (pH 7) with 150 mM NaCl.

As seen in figure B.1, only capacitive current 'envelope' was observed in the given voltammogram. This current is comparable to the capacitive current observed during measurement with mixed monolayer of probes and mercaptohexanol. No faradaic peaks were present within the same potential window as used to observe methylene blue peak. Therefore it could be concluded that the backfilling agent did not undergo electroactivity within the used potential window.
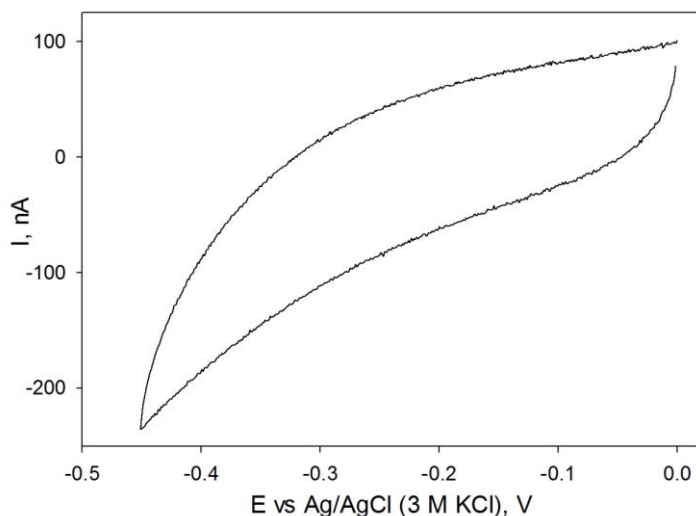

Fig B.1. Cyclic voltammogram of gold electrode modified with mercaptohexanol monolayer. Measurement was done in 20 mM PBS (pH 7) with 150 mM NaCl. Scan rate: 0.1 V s^{-1}.

To further observe the role of the backfilling agent, another measurement was performed. Similar to the gold electrode characterization experiment in chapter 5, the mercaptohexanol-modified electrode was interrogated in presence of diffusing redox mediator. Same electrode was then run in deaerated solution of 1 mM $K_3Fe(CN)_6$ with 100 mM KCl as supporting electrolyte. The obtained cyclic voltammogram is presented in figure B.2, overlaid with the voltammogram of bare gold electrode in identical situation (also presented in figure 6.4).

The voltammogram peaks of the mercaptohexanol-modified electrode had significantly higher peak separation (0.23605 ± 0.017 mV), when compared to the bare electrode's voltammogram peaks (0.06984 ± 0.00598 V). This was attributed to the insulating property of the mercaptohexanol. Electron transfer could not happen as easily with the extra layer of insulation on the electrode, as also put forward in chapter 5. Therefore more energy was required to drive the redox reaction, leading to a higher peak separation.
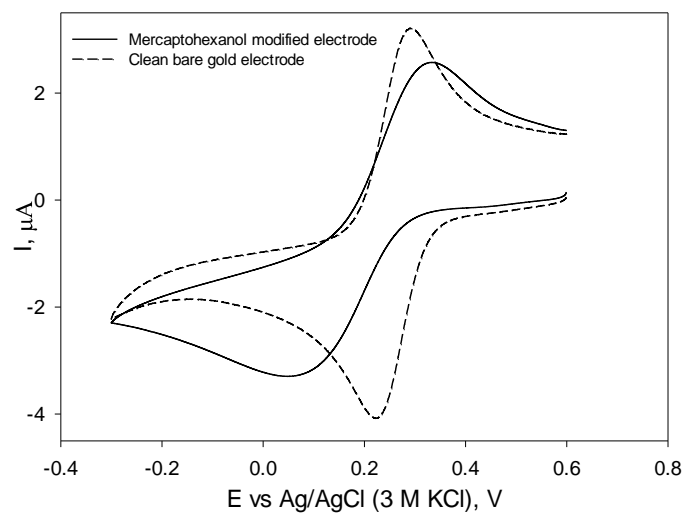
Fig B.2. Cyclic voltammogram of gold electrode modified only with mercaptohexanol monolayer, overlaid with voltammogram of clean bare gold electrode as in figure 6.4. Measurement was done in presence of 1 mM $K_3Fe(CN)_6$/100 mM KCl. Scan rate: 0.1 V s^{-1}.

2.   Electrode Modification Study

This appendix presents the results of electrode modification study. Three different monolayer assembly methods were studied and compared: the conventional two-steps, the inverse two-steps, and coadsorption. Experiments used a 20-nucleotide MB-labelled probe, to be immobilized on clean bare gold disk electrodes. All methods were performed using the same probe amount/concentration to have a clear comparison.

Conventional two-steps method protocol, included in appendix C, begins with deposition of thiolated probes unto the gold surface. After 16 hours incubation, the second step of modification followed. This time thiolated backfilling agent is incubated for 30 minutes. Electrodes were then interrogated with cyclic voltammetry to characterize its modified surface. Fig B.3 shows the CV obtained for electrodes modified using the conventional two-steps method. CV shows clear faradaic peaks in the redox potential range of methylene blue.
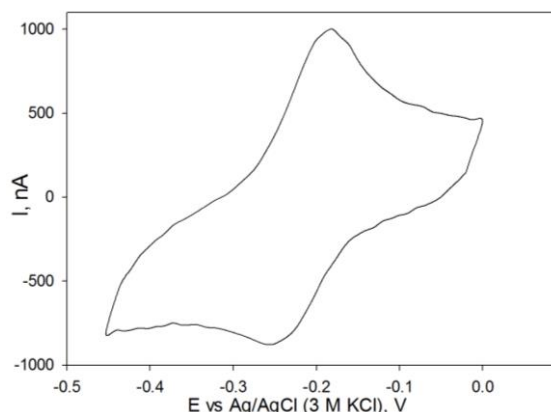

Fig B.3. Cyclic voltammogram of gold electrode modified with DNA probe/mercaptohexanol mixed monolayer through the conventional two-steps method. Measurement was done in 20 mM PBS (pH 7) with 150 mM NaCl. Scan rate: 5 V s⁻¹.

Inverse two-steps method protocol being with deposition of backfilling agent, followed by deposition of the probes. This method output CV as given in fig B.4.a. It was apparent that mainly capacitive current envelope was measured, no clear faradaic current was observed. Coadsorption assembly is an optimized method, which deposits both probes and backfilling agent in one deposition solution. Coadsorption CV result can be seen in fig B.4.b.
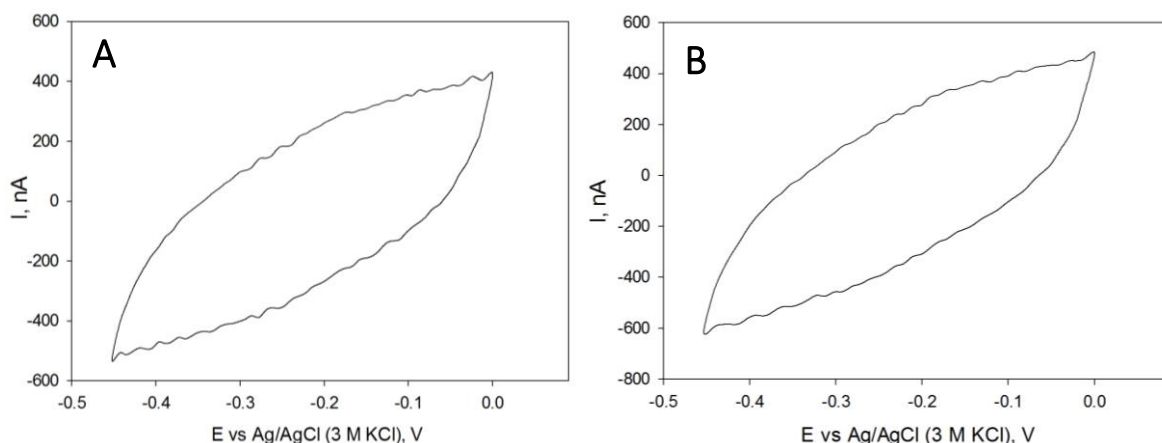

Fig B.4. (A) Cyclic voltammogram of gold electrode modified with DNA probe/mercaptohexanol mixed monolayer through inversed two-step immobilization method. Measurement was done in 20 mM PBS (pH 7) with 150 mM NaCl. Scan rate: 5 V s⁻¹.

(B) Cyclic voltammogram of gold electrode modified with DNA probe/mercaptohexanol mixed monolayer through coadsorption immobilization method. Measurement was done in 20 mM PBS (pH 7) with 150 mM NaCl. Scan rate: 5 V s^{-1}.

It was apparent that electrodes modified with inverse two-steps and coadsorption failed to adsorp enough probes to induce observable methylene blue signal. All methods used the same 10 μM probe concentration, a high enough concentration for such purpose. Therefore the conventional two-steps method proved to the most resource-efficient method. Similarly, for resource-efficiency, no further study was done in the other two immobilization techniques. All genosensors fabricated in the project were modified using the conventional two-steps modification method.

3.   Control Experiments

a)   Degradation control experiments

This experiment was done to verify that the signalling was induced by the presence of complementary target strands, as well as to evaluate the bioreceptor monolayer robustness. 4 electrodes were equivalently prepared for each sensor. Freshly modified electrodes were interrogated with DPV in 20 mM PBS buffer (pH 7) containing 150 mM NaCl. Then the electrodes were incubated with DNA-free PBS buffer (pH 7) containing 150 mM NaCl and 5 mM $MgCl_2$, same buffer for hybridization with complementary strands, for 1 hour. The electrodes were then interrogated again.

Results given in fig B.5 show that incubation with DNA-free buffer introduced negligible change in DPV signal. All fabricated sensors responded in similar way (other results not shown). Therefore it can be safely concluded that the used buffer did not induce the observed sensor response. It also revealed that interrogation does not degrade the sensor monolayer, as repeated measurement output comparable response.
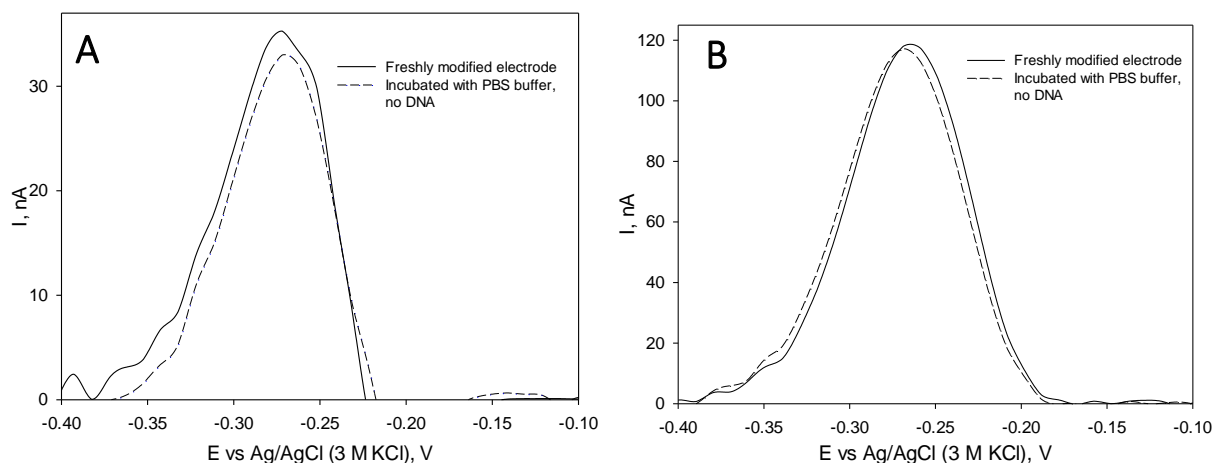

Fig B.5. Differential pulse voltammogram of (a) syntheticDNA MB-tagged probes (b) hsa-mir-618 MB-tagged probes. Freshly modified DPV is overlaid with DPV of electrode after incubation DNA-free 20 mM PBS buffer (pH 7) containing 150 mM NaCl and 5 mM $MgCl_2$ for 1 hour. DPV protocol is as presented in Appendix C.4.

b)   Specificity control experiment

Similarly, specificity of the sensors were also evaluated experimentally. 4 electrodes were equivalently prepared for each sensor. Freshly modified electrodes were interrogated with DPV in 20 mM PBS buffer (pH 7) containing 150 mM NaCl. Then the electrodes were incubated with 10 µL of 2 µM non-cognate DNA solution in PBS buffer (pH 7) containing 150 mM NaCl and 5 mM $MgCl_2$, for 30 minutes. SyntheticDNA sensors were incubated with hsa-mir-618 target DNA, and vice versa, as they do not have complementary parts. After incubation, the electrodes were then interrogated again.

Results given in fig B.6 show that when challenged with non-cognate DNA in excess, negligible change in DPV signal was observed. All fabricated sensors responded in similar way (other results not shown). This verified the specificity of the bioreceptor in ~150 times excess of non-specific DNA strands.
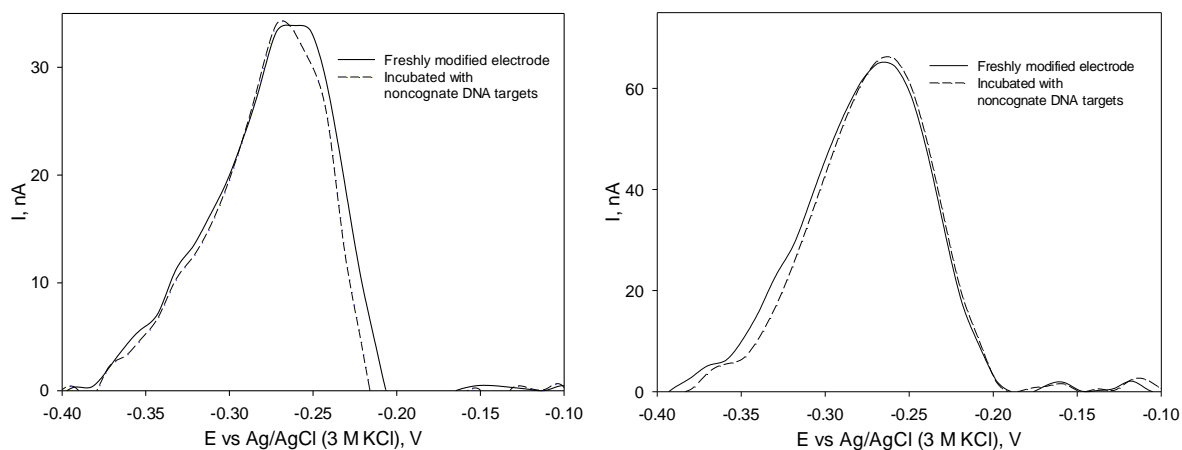
Fig B.6. Differential pulse voltammogram of (a) syntheticDNA MB-tagged probes (b) hsa-mir-618 MB-tagged probes. Freshly modified DPV is overlaid with DPV of electrode after incubation with 10 μL of (a) 2 μM has-mir-618 target probes (b) 2 μM cSyntheticDNA target probes in 20 mM PBS buffer (pH 7) containing 150 mM NaCl and 5 mM MgCl₂ for 30 minutes. DPV protocol is as presented in Appendix c.4, sequences are as presented in table 7.1.

4.   Regeneration

This part contains the results of regeneration of the fabricated sensors.

a)   Regeneration of syntheticDNA sensors

Fig B.7 compares the DPV of a synthetic DNA sensor, when it was freshly modified, after incubation with high concentration of target strands, and after dehybridization. Dehybridization was achieved by rinsing electrode surface with room temperature Milly-Q water for 40 seconds.
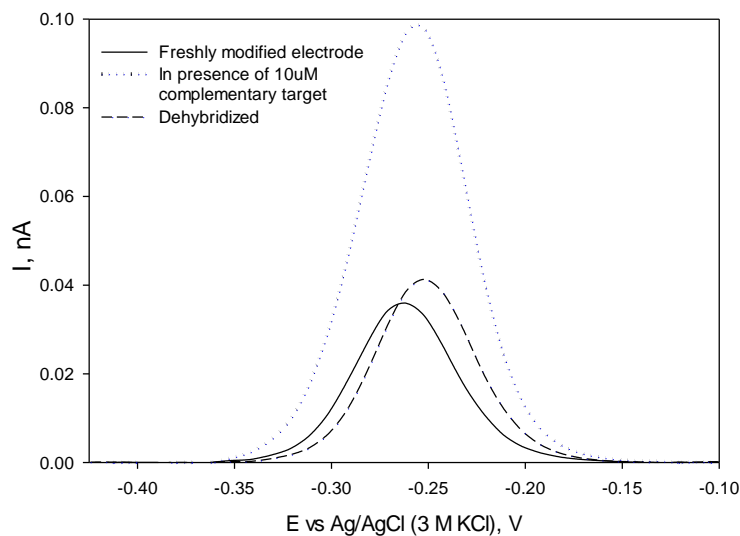

Fig B.7. Differential pulse voltammograms of syntheticDNA sensors. Dehybridized signal is overlaid with blank and in presence of the highest concentration complementary target.

b)   Regeneration of miRNA sensors

Fig B.8 compares the DPV of a hsa-mir-618 miRNA sensor, when it was freshly modified, after incubation with high concentration of target strands, and after dehybridization. Dehybridization was achieved by rinsing electrode surface with room temperature Milly-Q water for 40 seconds.
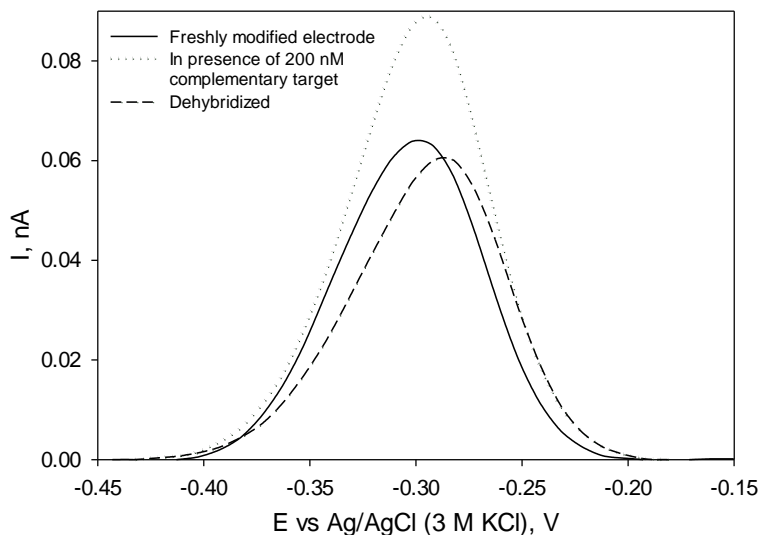

Fig B.8. Differential pulse voltammograms of microRNA sensors. Dehybridized signal is overlaid with blank and in presence of the highest concentration complementary target.

5. Kinetics Study

As mentioned in chapter 7, peak currents from the modulated scan rates were used to study the kinetics of the electrode processes. The figures below plot the peak currents against the scan rates or square root of scan rates. Linear line was fitted to each plot, with the coefficient of determination (R^2, calculated by equation B.1) given for each fitting. This coefficient expresses the proportion of the change in the peak current attributable to the change in scan rates or square root of scan rates. The higher the value of R^2, the more correlated the two changes are.

$$R^2 = \left(\frac{\sum(x - \bar{x})(y - \bar{y})}{\sqrt{\sum(x - \bar{x})^2(y - \bar{y})^2}} \right)^2 \qquad\qquad (\text{B.1})$$

Fig B.9 plots the peak currents of the synthetic DNA probes in absence of the target DNA, against the scan rates (A) and against the square root of scan rates (B). Both correlation had noticeably high R^2 values (caused by the very close relation between scan rate and square root of square rate). Therefore it was imperative to analyse them in comparison rather than in their absolute R^2 values. For fig B.9, the peak currents were more correlated directly with scan rates, rather than its square root values. This suggested that the electrode process was more governed by a confined redox species than by diffusion.
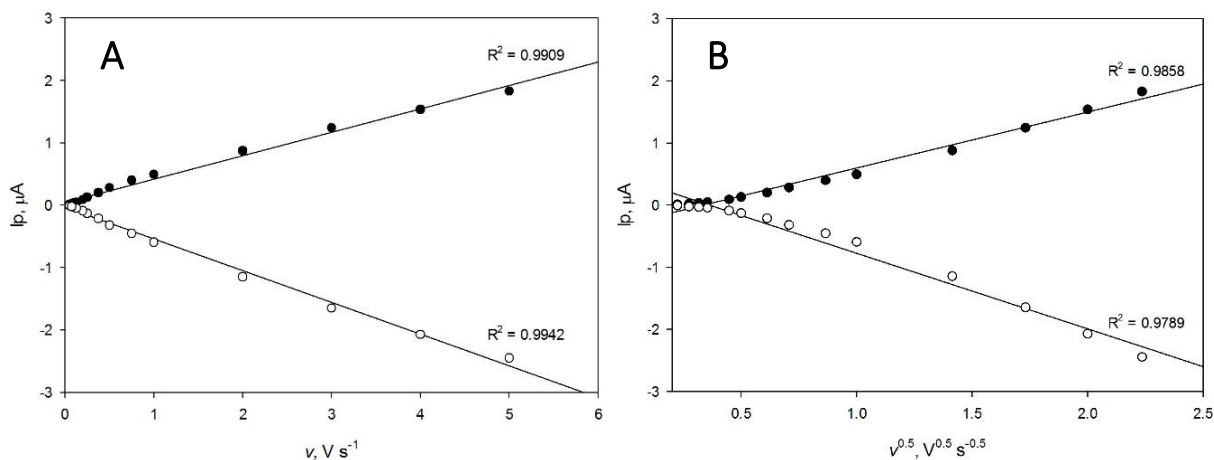

Fig B.9. Representative results of hairpin DNA structure (in no presence of target DNA)

Similarly, same study was done for the hybridized DNA, with results shown in fig B.10. In contrast, the peak currents obtained were more correlated to the square root of scan rates than to the scan rates. This suggested that the electrode process was governed by diffusion, which means that the redox probe was not confined on the electrode surface anymore (assumedly through the hybridization).
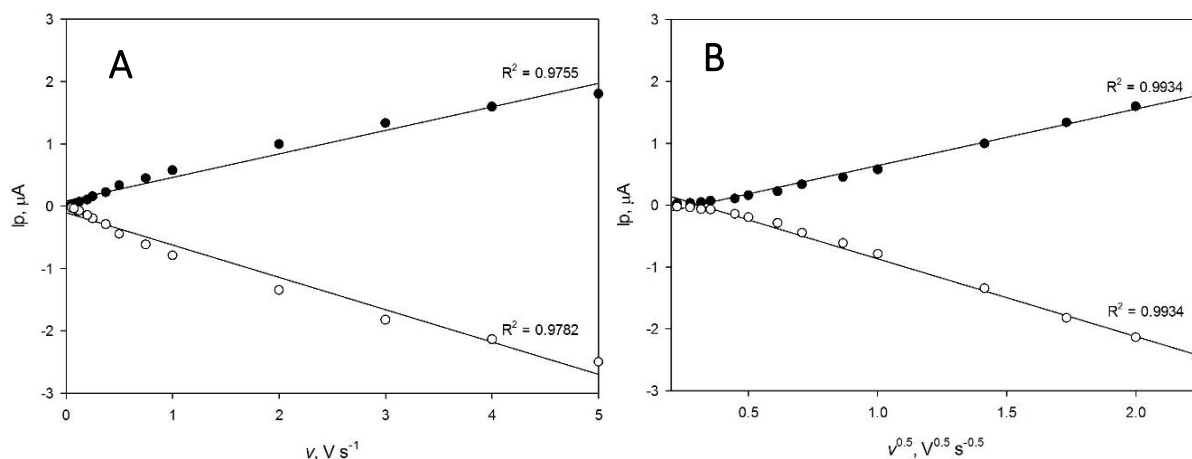
Fig B.10. Representative results of duplex DNA structure (in presence of 10 μM target DNA)

It is noteworthy that not all of the probes conform identically at all time. I.e. not all probes are in stem-loop structure when unhybridized/in absence of target strands and not all probes are hybridized in presence of target strands. This limits the absolute accuracy of the model/study explained above, since in both cases the electrode processes are not governed one sovereign process. Therefore the model was used in strictly relative term, mostly to observe the change between processes before and after introduction of target strands. Even then, big variance was observed between electrodes from time to time.

Appendix C
Protocols

1.　Buffer Preparation Protocol

PBS -> osmolarity and ion concentrations are isotonic and non-toxic even to cells -> physiologically-relevant

All material is purchased from Sigma-Aldrich, Germany.
To make: ~200 mL of 20mM phosphate buffered saline (pH 7.0) with 0.15 M NaCl
1. In one flask, dissolve the following in 100 mL Milli-Q water:
    174.18 g/mole x 0.020 mol/L x 0.100 L = 0.34836 g of K_2HPO_4 (dibasic salt)
    58.44 g/mole x 0.150 mol/L x 0.100 L = 0.8766 g of NaCl
2. In another flask, dissolve the following in 100 mL Milli-Q water:
    136.09 g/mol x 0.020 mol/L x 0.100 L = 0.27218 g of KH_2PO_4 (monobasic salt)
    58.44 g/mol x 0.150 mol/L x 0.100 L = 0.8766 g of NaCl
3. Adjust pH, by adding the monobasic salt solution little by little to the dibasic salt solution:
    Start with the dibasic salt solution, stirred, and monitored by pH meter.
    Add the monobasic salt solution little by little (around 1 mL) to the solution.
    Continuously monitor the pH, stop adding when it reaches 7.0.
    Transfer buffer to storage bottle.

To make: ~200 mL of 20mM phosphate buffered saline with 150 mM NaCl and 5 mM $MgCl_2$
1. In one flask, dissolve the following in 100 mL Milli-Q water:
    174.18 g/mol x 0.020 mol/L x 0.100 L = 0.34836 g of K_2HPO_4 (dibasic salt)
    58.44 g/mol x 0.150 mol/L x 0.100 L = 0.8766 g of NaCl
    95.21 g/mol x 0.005 mol/L x 0.100 L = 0.047605 g of $MgCl_2$
2. In another flask, dissolve the following in 100 mL Milli-Q water:
    136.09 g/mol x 0.020 mol/L x 0.100 L = 0.27218 g of KH_2PO_4 (monobasic salt)
    58.44 g/mol x 0.150 mol/L x 0.100 L = 0.8766 g of NaCl
    95.21 g/mol x 0.005 mol/L x 0.100 L = 0.047605 g of $MgCl_2$
4. Adjust pH, by adding the monobasic salt solution little by little to the dibasic salt solution:
    Start with the dibasic salt solution, stirred, and monitored by pH meter.
    Add the monobasic salt solution little by little (around 1 mL) to the solution.
    Continuously monitor the pH, stop adding when it reaches 7.0.
    Transfer buffer to storage bottle.

2. Electrode Modification Protocol

a) DNA probe hairpin immobilization through conventional two-steps self-assembly

1. (If necessary) Dilute 0.5 M TCEP (tris-(2-carboxyethyl)-phosphine) to have 0.5 mM TCEP.
   Take 1 µL of 0.5 M TCEP, add 999 µL of buffer (typically, deposition buffer: 20 mM PBS (pH 7) with 150 mM NaCl).
2. To be drop-casted on each electrode: 10 µL of 10 µM DNA solution.
   Calculate the amount of DNA stock solution necessary to achieve the said solution:
   e.g. DNA stock solution concentration = 100 µM
   $C_1 V_1 = C_2 V_2$; 100 µM V_1 = 10 µM x 10 µL ; V_1 = 1 µL of DNA stock solution
3. In a 0.5 mL tube, put the calculated amount of DNA stock solution, add 1 µL of 0.5 mM TCEP.
   Centrifuge and vortex tube, let for 1 hour reaction time in room temperature, protected from light (when probe has methylene blue or other light sensitive moiety).
4. After reaction time, add buffer to bring total solution volume to 10 µL
   i.e. stock solution volume + TCEP volume + buffer volume = 10 µL
5. Take 10 µL of the solution, drop cast it on the gold electrode (held upside down on a polystyrene block).
   Cover with 1.5 mL tube to avoid evaporation, cover with aluminium foil to protect from light.
   Leave for self-assembly in room temperature.

b) DNA duplex immobilization through conventional two-steps self-assembly

1. (If necessary) Dilute 0.5 M TCEP (tris-(2-carboxyethyl)-phosphine) to have 0.5 mM TCEP.
   Take 1 µL of 0.5 M TCEP, add 999 µL of buffer (typically, deposition buffer: 20 mM PBS (pH 7) with 150 mM NaCl).
2. To be drop-casted on each electrode: 10 µL of 10 µM DNA probe with 15 µM (complementary) target DNA.
   Calculate the amount of DNA stock solution necessary to achieve the said solution:
   e.g. Probe DNA stock solution concentration = 100 µM
   $C_1 V_1 = C_2 V_2$; 100 µM V_1 = 10 µM x 10 µL ; V_1 = 1 µL of DNA stock solution
   Complementary DNA stock solution concentration = 100 µM
   $C_1 V_1 = C_2 V_2$; 100 µM V_1 = 15 µM x 10 µL ; V_1 = 1.5 µL of DNA stock solution
3. In a 0.5 mL tube, put the calculated amount of DNA stock solution, add the calculated amount of complementary DNA stock solution, and add 1 µL of 0.5 mM TCEP.
   Centrifuge and vortex tube, let for 1 hour reaction time in room temperature, protected from light (when probe has methylene blue or other light sensitive moiety).
4. After reaction time, add buffer to bring total solution volume to 10 µL
   i.e. Probe DNA volume + complementary DNA volume + TCEP volume + buffer volume = 10 µL
5. Take 10 µL of the solution, drop cast it on the gold electrode (held upside down on a polystyrene block).
   Cover with 1.5 mL tube to avoid evaporation, cover with aluminum to protect from light.
   Leave for self-assembly in room temperature.

3. Backfilling Protocol

1. Wash the modified electrodes by soaking them in 0.5 mL buffer (20 mM PBS (pH 7)/0.150 M NaCl) for 5 minutes
2. Prepare 2 mM mercaptohexanol (NC$_6$OH [134.29 g mol^{-1}, ρ = 0.981 g mL^{-1}], Sigma-Aldrich, Germany) in buffer in two steps: first to make 10 mM solution, then dilute it to 2 mM solution.
   134.29 g/mol x 0.100 mol/L x 0.001 L = 1.3424 x 10^3 g
   1.3424 10^3 g/0.981 g/mL = 1.368 µL
3. *(Do inside the fume hood! Check MSDS!)*
   In a 1.5 mL tube, transfer 1.368 µL of mercaptohexanol stock solution.
   Add 998.632 µL of buffer. Shake rigorously for ~1 minute. This makes the 10 mM mercaptohexanol solution.
4. Transfer 200 µL of the 10 mM mercaptohexanol solution into another 1.5 mL tube.
   Add 800 µL of buffer. Shake rigorously for ~1 minute. This makes the 2 mM mercaptohexanol solution.
5. Take 10 µL of 2 mM mercaptohexanol solution, drop cast it on the electrode surface (held upside down on a polystyrene block).
   Cover and protect from light with a 1.5 mL tube. Leave for self-assembly for 30 minutes in room temperature.
6. After 30 minutes, wash the backfilled electrodes by soaking in 0.5 mL buffer for another 5 minutes.
7. Transfer electrodes to new tube with 0.5 mL buffer (they can be taken out of the fume hood).
   After being soaked for another 5 minutes, electrodes are ready.

4. Calibration Protocol (hairpin beacon with tethered methylene blue)

- DPV Protocol (reduction)
  Modulation amplitude: 40 mV
  Step potential: -10 mV
  Scan rate: 20 mV s^{-1} (Interval time: 0.5 s)
  Initial potential: 0 V
  End potential: -0.45 V

  nb. Methylene blue must be reduced first, before it can be oxidized.

- DPV Protocol (oxidation)
  Modulation amplitude: 40 mV
  Step potential: 10 mV
  Scan rate: 20 mV s^{-1} (Interval time: 0.5 s)
  Initial potential: -0.45 V
  End potential: 0 V

- CV Protocol
  Start potential: 0 V
  Upper vertex potential: 0 V
  Lower vertex potential: -0.45 V
  Stop potential: -0.001 V
  Step potential: -0.001 V
  Scan rate: 0.1 V/s (may be varied to obtain kinetics information)

1. In electrochemical cell, deaerate electrolyte (20 mM PBS (pH 7)/0.15 M NaCl) by bubbling it with argon for at least 5 minutes. Blanket the solution with argon afterwards (also during measurement).
2. Put in the modified working electrode. Run measurements of interest.
3. After measurements, take out the working electrode. Bubble the electrolyte with argon again.
4. Slightly rinse the working electrode. Cast 10 µL drop of the target strand solution (starting from the lowest concentration) on top of the electrode surface (held upside down on a polystyrene block).
   Cover with 1.5 mL tube, protect it from light with aluminum foil. Incubate in room temperature for 30 minutes.
5. Gently flick the electrode after incubation to get rid of the incubating drop. Electrode is ready for measurement (step 1-3).
6. Repeat for the steps for other concentrations of interest.